AD

Research and Development Technical Report
ECOM - 0056 - F

TRANSIENT METHODS FOR ANALYSIS OF ELECTROCHEMICAL KINETICS

FINAL REPORT
by
JORGE E. A. TONI
DECEMBER, 1969

CONTRACT NO. DAAB07-69-C-0056

BATTERY CORPORATION OF AMERICA
RED BANK, NEW JERSEY

ECOM
UNITED STATES ARMY ELECTRONICS COMMAND · FORT MONMOUTH N.J.

96

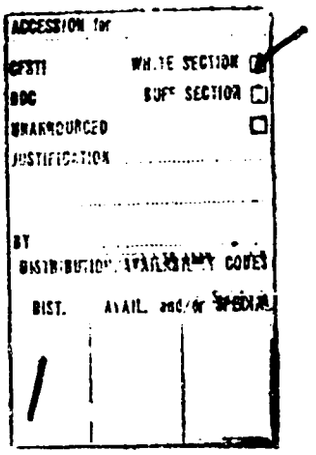

NOTICES

DISCLAIMERS

The findings in this report are not to be construed as an official Department of the Army position, unless so designated by other authorized documents.

The citation of trade names and names of manufacturers in this report is not to be construed as official Government indorsement or approval of commercial products or services referenced herein.

DISPOSITION

Destroy this report when it is no longer needed. Do not return it to the originator.

Reports Control Symbol
OSD-1366

December, 1969

Technical Report ECOM-0056-F

TRANSIENT METHODS FOR ANALYSIS OF ELECTROCHEMICAL KINETICS

FINAL REPORT

October 1, 1968 to September 30, 1969

Contract No. DAAB07-69-C-0056

Jorge E. A. Toni

BATTERY CORPORATION OF AMERICA
43 West Front Street
Red Bank, New Jersey

For

U. S. Army Electronics Command, Fort Monmouth, New Jersey

TABLE OF CONTENTS

	Page
ABSTRACT	1
INTRODUCTION	2
A. REVIEW OF RELAXATION TECHNIQUES	5
B. INSTRUMENTATION	26
C. CHARACTERIZATION OF MERCURY BATTERIES BY PULSE TECHNIQUES	31
D. THE ELECTROCHEMICAL REDUCTION OF m-DINITRO-BENZENE (m-DNB) IN MAGNESIUM PERCHLORATE SOLUTIONS	44
E. THE ELECTROCHEMICAL OXIDATION OF ZINC METAL	67
F. DISSOLUTION RATE MEASUREMENT	87
REFERENCES	88

TABLE OF FIGURES

Figure Number		Page
1.	Potential Step Method	6
2.	Cyclic Potentiostatic Method	10
3.	Current Step Method	12
4.	Cyclic Galvanostatic Method	15
5.	Double Pulse Galvanostatic Method	17
6.	Overpotential Time Response in Double Pulse Galvanostatic Method	18
7.	Ring-Disc Electrode Circuit - No. I	27
8.	Ring-Disc Electrode Circuit - No. II	28
9.	Potentiostatic System with IR Compensation	30
10.	Circuit Diag. for Reference Electrode Testing	32
11.	Behavior of the $Cd/Cd(OH)_2$ Electrode	33
12.	Location of the Reference Electrode in a Mercury Battery	35
13.	Galvanostatic Experiment with Mercury Battery	37
14.	Overpotential Time Response of Mercury Battery Electrodes	40
15.	Application of Impedance Transformation Data Method	41
16.	Overpotential Time Response of the Electrodes of a Severely Discharged Mercury Battery	43
17.	Cyclic Voltammograms of m-DNB	47
18.	Cyclic Voltammogram of m-DNB-PGE	49
19.	pH Effect	50
20.	Scan Rate Effect	52
21.	Scan Rate Effect	53
22.	Rotation Rate Effect	55
23.	Rotation Rate Effect	57

Figure Number		Page
24.	Determination of Rate Constant	59
25.	Potentiostatic Method	61
26.	Ring-Disc Electrode Experiments	63
27.	Ring-Disc Electrode Experiments	64
28.	Effect of Reversal Potential	68
29.	Sweep Rate Effect	71
30.	Effect of Reversal Potential	73
31.	Non-Amalgamated Zinc.Stirred Solutions	75
32.	Amalgamated Zinc.Stirred Solutions	77
33.	Ring-Disc Electrode Experiments	79
34.	Effect of Rotation Rate on Peak Current	82
35.	Collection Efficiency of Amalgamated and Non-Amalgamated Electrodes	83
36.	Passive Region	85

ABSTRACT

Perturbation of the equilibrium state of electrochemical systems included the following techniques: relaxation methods, techniques with linearly varying potential, hydrodynamic methods (under well controlled forced correction) and techniques employing carbon paste electrodes of insoluble electroactive materials.

This final report includes a review of relaxation methods and describes the principal achievements in the following areas: Instrumentation: Two new circuits for the independent control of two working electrodes (ring-disc assemble) in the same electrolyte are described; Characterization of mercury batteries by pulse techniques: It was proved that pulse methods can give promising results concerning the state of charge of mercury batteries; Electroreduction of m-dinitrobenzene: The mechanism of m-DNB reduction in $Mg(ClO_4)_2$ solution correspond to an ECECE mechanism. An electrode mechanism consistent with the experimental data was postulated; Oxidation of zinc anode; The evaluation of oxidation and reduction processes of zinc gave supporting data for an "adsorption model" instead of the classical "dissolution-precipitation model" assigned to the passivation of zinc anode; Dissolution rate measurement: Utilizing the rotating ring-disc electrode concept, a new theory for the measurement of dissolution and corrosion rates was developed.

INTRODUCTION

This final report includes the summary of our research work during the period of October 1, 1968 to September 30, 1969. During this period, we did explore and applied different fields in transient methods related with electrode processes. We have analysed, developed and applied novel electrochemical techniques, involving ourselves in methods controlled by diffusion or forced convection and under closed or open circuit conditions. We were led to create new instrumental devices appropriate to the requirements of the techniques investigated, and we were able to prove their capabilities by resolving representative electrode processes.

Our work included a great variety of electrochemical techniques under different mass control conditions and under perturbation or recovery of the equilibrium state. These methods may be grouped in the following way:

I. Methods involving linear variation of the imposed potential with time.

One should include here the diffusion controlled techniques known as Linear Sweep Voltammetry and Cyclic Voltammetry. They generate typical current-potential or current-time curves as a consequence of the perturbation of the equilibrium of the electrochemical system under well defined potentiostatic conditions. They have shown enormous possibilities in the diagnosis of electrode process mechanism which are controlled by surface, diffusion and/or kinetic chemical factors. Typical examples are their application in the electrode mechanism studies of the m-dinitrobenzene reduction and in the electrochemical oxidation of zinc-metal. By application of these methods, in different fashions and following specific trends, we were able to interpret the reduction steps of m-dinitrobenzene and postulate a mechanism. In the oxidation of zinc, experiments with linearly varying potential per-

mitted a clear evaluation of the two passivation processes. But to be able to use these methods to their maximum possibilities, we had to improve the capabilities of the available potentiostats, by design and fabrication of fast IR compensation systems.

II. Relaxation Methods

These techniques were reviewed and reevaluated. We concluded that open-circuit recovery techniques should be brought to the attention of fast charge transfer electrode studies. The application of equivalent electrical analogs is simplified in decay methods by the elimination of the cell resistance and the consequent series model approach. Analysis by Laplace transformation was included with promising advantages. Examples of the application of these techniques can be found in our research relative to mercury batteries.

III. Convective Methods

They include the methods developed under mass transfer by forced convection. Principally, we worked with rotating disc electrodes and with the combination of a rotating disc surrounded by a ring electrode. These methods are of incalculable value; they permit combinations of almost any other technique under perfectly controlled and reproducible conditions of a convective-diffusion layer. The ring-disc electrode offers the great advantage of having two independent working electrodes in the same media and consequently, permits the simultaneous transient study of an electrode reaction (occuring on the disc) by another electrochemical system, (ring). Examples of our work with convective methods are: the development of dissolution rate measurements, the determination of the rate constant for the chemical reaction coupled in the ECE mechanism of m-dinitrobenzene, and the ideas developed in the passivation model of the zinc anode.

Convective methods required also, a great effort in development of instrumentation. We have created and successfully employed two new electrical circuits for the independent control of two or more working electrodes under potentiostatic or galvanostatic conditions.

IV. Carbon Paste Electrodes

The fundamental studies of insoluble electroactive materials suffer serious experimental difficulties. The use of carbon paste electrodes mixed with the electroactive substance may open new possibilities in the field of porous electrodes. Manganese dioxide and m-dinitrobenzene were chosen for the electrode evaluation by diffusion and convection control transient methods. It is expected that if the electrochemical reaction takes place within and at the surface of the crystals, they should be influenced by the factors controlling the nature of the crystals and their contact with the solution. Porous effects must play an important role in the overall behavior. The initial experimental data was really promising, but the lack of theoretical work in the electrochemical behavior of this type of electrode makes the interpretation of results difficult. The starting point should be the development of this theory.

In the following pages, we are going to describe specifically, each of the major projects developed during the contract, which will prove the statements expressed above.

A REVIEW OF RELAXATION TECHNIQUES

The term "relaxation" applies to both pulse and decay methods and describes the process of gradual change of a physical system from a non-equilibrium to an equilibrium state. The process involves equalization, by diffusion, of unequal reactant concentrations at the electrode surface. Pulse methods involve the study of electrode kinetics during a perturbation, whereas, decay methods involve the study of electrode kinetics after the perturbation has been removed.

a) POTENTIOSTATIC METHODS

1. Potential Step Method: This method was first proposed by Gerisher and Vielstich[1]. In this method, the electrode potential is suddenly changed from its equilibrium value Ee, to some other value E_1 (Fig. 1). The resulting current is measured as a function of time (Fig. 1a). The expression for the current density, neglecting the effect of double-layer charging and considering a simple electron transfer without kinetics complications, is given by the following equation:

$$i = nF\left(C_o^{\circ} k_1 - C_R^{\circ} k_2\right) \xi\left(Q\sqrt{t}\right) \qquad (1)$$

where $$k_1 = \frac{i_o}{nFC_o^{\circ}} \exp\left[-\frac{\alpha nF(E_1 - E_e)}{RT}\right]$$

$$k_2 = \frac{i_o}{nFC_R^{\circ}} \exp\left[\frac{(1-\alpha) nF(E_1 - E_e)}{RT}\right]$$

$$\xi\left(Q\sqrt{t}\right) = \exp\left(Q^2 t\right) \operatorname{erfc}\left(Q\sqrt{t}\right)$$

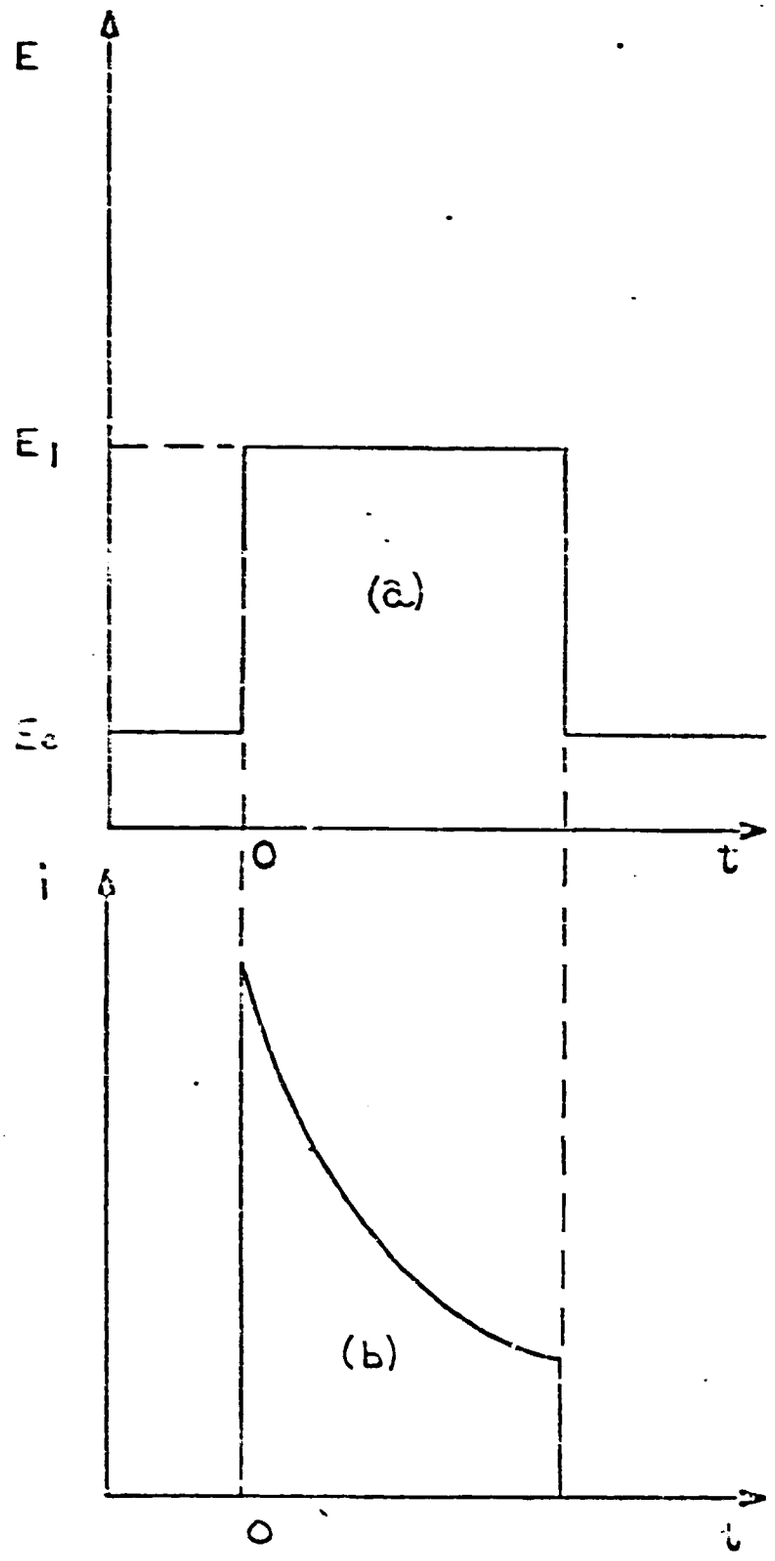

FIGURE 1

POTENTIAL STEP METHOD

$$Q = \frac{k_1}{\sqrt{D_O}} + \frac{k_2}{\sqrt{D_R}}$$

C_o° = Conc. of oxidized form in the bulk of solution

C_R° = Conc. of reduced form in the bulk of solution

$E_1 - E_e = \eta$ = overpotential

α = transfer coefficient

i_o = exchange current density

$$i_o = nFk^\circ (C_o^\circ)^{1-\alpha} (C_R^\circ)^{\alpha} \qquad (2)$$

k° = rate constant at equilibrium potential

The combination of equations (1) and (2) depends on k° and may therefore, in principle, be used for the calculation of this quantity from experimental i-t curves. However, this expression is extremely complicated for practical use. Therefore, several simplifications can be made for the calculation of k° and α. Assuming small potential changes ($\eta \ll RT/F$) and short time intervals ($Q\sqrt{t} \ll 1$), we obtain the following approximate expression for current density:

$$i \cong -i_o \frac{nF(E-E_e)}{RT} \left(1 - \frac{2Q}{\sqrt{\pi}} \sqrt{t}\right) \qquad (3)$$

Thus, a plot of i as a function of $\sqrt{t}$ should be a straight line. Extrapolation to t=0 results in the quantity $-\frac{i_o nF\eta}{RT}$ from which it is easy to obtain i_o. In order to determine α, measurements are carried out for different concentrations of C_o° at C_r° = constant and the exchange curren

densities are found for each concentration. It follows from equation (2) that

$$\log i_o = \overbrace{\log (nFk^\circ) + \alpha \log C_R^\circ}^{\text{constant}} + (1-\alpha) \log C_o^\circ$$

By plotting log i_o as function of log C_o^o, we obtain a straight line, the slope of the line is equal to $(1 - \alpha)$. Once α is known, it is then easy to calculate k° from equation (2).

2. Voltage Step Method: The potential step method required the use of a potentiostat. Simpler instrumentation can be used if only a constant potential difference (voltage) in the cell is maintained. Vielstich and Delahay[2] proposed this modification which was called "voltage step method". In this case, the potential of the working electrode varies because the current and therefore, the ohmic drop $\Delta E_{ohmic} = I R_t$ varies; R_t = total resistance of the circuit. Thus:

$$E_i - E_e + I R_t = V$$

where V = circuit voltage.

The changes of the voltage and the current versus time, are similar to those shown in Fig. 1. The equation for the current, following assumptions similar to those in the previous case is expressed by:

$$I \cong i_o A \frac{nFV}{RT} \cdot \frac{1}{\beta+1} \left(1 - \frac{2Q_1\sqrt{t}}{\sqrt{\pi}}\right)$$

Where:

$$\beta = \frac{i_o A R_t n F}{RT}$$

$$Q_1 = \frac{i_o N}{\beta+1}$$

$$N = \frac{1}{nF}\left(\frac{1}{C_o^\circ \sqrt{D_o}} + \frac{1}{C_R^\circ \sqrt{D_R}}\right)$$

A = area of electrode

The determination of i_o; β' and α follows the same procedure discussed in the potential step method.

3. The Cyclic Potentiostatic Method: This method was proposed by Smit and Wijmen[3]. The electrode potential changes as shown in Fig. 2a and the current has the pattern of Figure 2b.

The first half-cycle is identical to the potential step method. In the second half-cycle, the current is reversed and behaves similarly (but not necessarily symmetrically) to the first half-cycle. The derivation for the cyclic current is considerably more complicated than for previous cases. The expression for the absolute value of the cyclic current may be written as follows:

$$|i(\theta)| = nF\left\{C^{\circ}\left[k_1(E_1) - k_1(E_2)\right] - C_e^{\circ}\left[k_2(E_1) - k_2(E_2)\right]\right\} \chi(s,\theta) \qquad (4)$$

where $\chi(s,\theta)$ is some function of s and θ given by:

$$\chi(s,\theta) = \sum_{p=0}^{\infty}\left[\Xi\left(s\sqrt{p+\theta}\right) - \Xi\left(s\sqrt{p+0.5+\theta}\right)\right]$$

$$\theta = t/T \quad ; \quad s = Q\,t^{1/2}$$

The method includes several instrumentation artifices which permit the comparison of both half-cycle currents. By varying E_2, while E_1 is kept constant, the current-time curves can coincide and under these conditions and if $E_1 - E_e$ are sufficiently negative and positive respectively, (> 100 mV) the following equation holds:

$$E_2 = \alpha'\left(E_2 - E_1\right) - \left[E_e - \frac{RT}{2nF}\ln\frac{D_R}{D_O}\right]$$

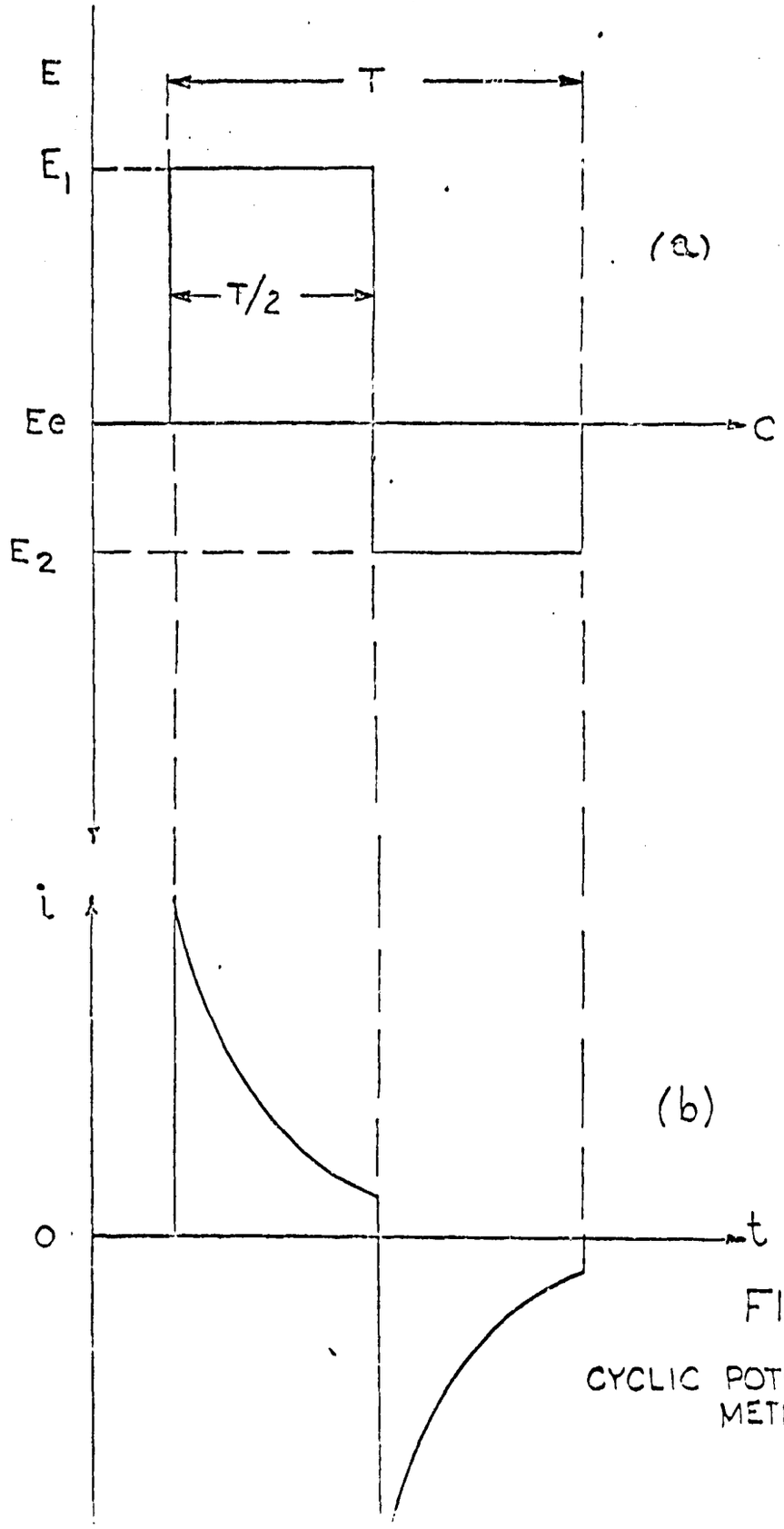

FIGURE 2

CYCLIC POTENTIOSTATIC METHOD

By plotting E_2 as a function of $E_2 - E_1$, α can be determined. Now k° can be obtained using equation (4). Under the same conditions imposed above, the terms $k_1(E_2)$ and $k_2(E_1)$ may be neglected and the expression for the current density after the substitution of $k_1(E_1)$ and $k_2(E_2)$ becomes the following:

$$|i| = n F k^\circ \left\{ C_o^\circ \exp\left[\frac{\alpha n F (E_1 - E_e)}{RT}\right] + C_R^\circ \exp\left[\frac{(1-\alpha) n F (E_2 - E_e)}{RT}\right] \right\} L(s,t)$$

As $L(s,t)$ may be taken from tables, the k° constant can be calculated. The main advantage of the cyclic potentiostatic method as compared to the basic method lies in the rapid determination of kinetic parameters of the electrochemical reactions since, in this particular case, it is possible to carry out the measurements with only one concentration of the reactants.

b) GALVANOSTATIC METHODS

1. Current Step Methods: To some extent, galvanostatic methods are the reverse of potentiostatic methods; in galvanostatic methods the current is changed suddenly from zero to some given value, and the resulting variation of potential with time is recorded, Figure 3.

Since the absence of current corresponds to the equilibrium potential Ee, it is clear that the potential difference (IR-free) measured is the over-potential $\eta = E - Ee$. The current step method as a relaxation technique was proposed first by Berzins and Delahay[4]. The expression of η, as a function of t for $\eta \ll \frac{RT}{nF}$, is found to be

$$\eta = \frac{RT}{nF} i \left(\frac{2N}{\pi^{1/2}} t^{1/2} + \frac{1}{i_o} \right) \quad (5)$$

Where N has the same expression shown above. But this expression does not agree with the experimental data. In fact, the charging of the double

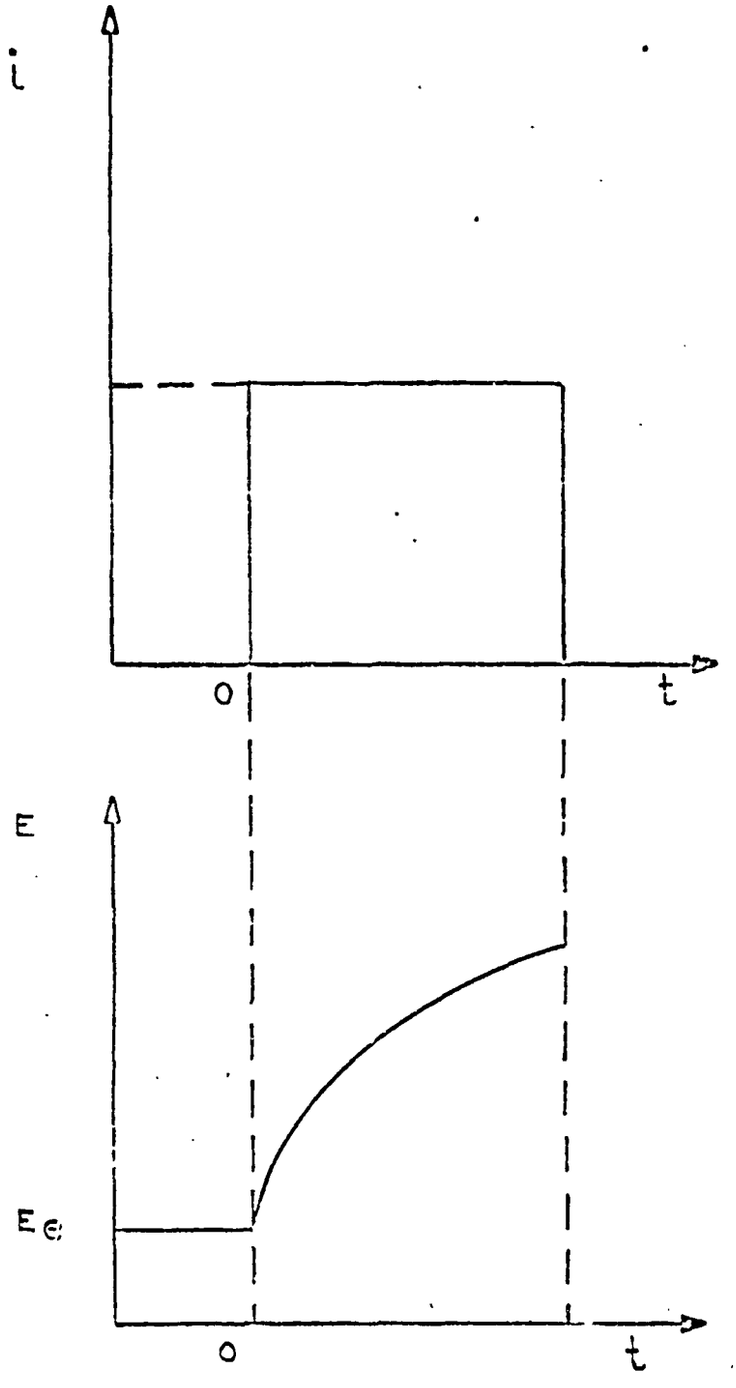

FIGURE 3

CURRENT STEP METHOD

layer was not taken into account in the derivation. In reality, it is the total current

$$i_t = i_f + i_c$$

i_f = faradaic current
i_c = charging current

which is forced to change stepwise. If the double layer capacity in the potential interval of interest is equal to Cd, then $i_c = C_d\left(\frac{d\eta}{dt}\right)$ and the faradaic current is given by $i_f = nFD_o\left(\frac{\partial C_o}{\partial x}\right)_{x=0}$. A rapid variation in overpotential is to be expected initially; therefore, $d\eta/dt$ is large and the charging current is large. Later, the overpotential increases much more slowly and the faradaic current predominates. In order to obtain the correct solution for the dependance of η on t, Berzins and Delahay [4] derived the following equation.

$$\eta \cong RT/nF \; i\left(\frac{2N}{\pi^{1/2}} t^{1/2} - \frac{RTN^2}{nF} C_d + \frac{1}{i_o}\right) \qquad (6)$$

The conditions include now that

$$\eta \ll RT/nF \quad \text{and} \quad t > 5\times10^{-5} \text{ sec}$$

From equation (6) it follows that the recorded potential variation consists of three parts: concentration polarization, the potential variation caused by the charging of the double layer and the electrochemical polarization. The calculations of kinetic reaction parameters from the experimental curves by equation (6) may be conveniently carried out as follows: The plot of $\eta - t^{1/2}$ is a straight line with the slope

$$\delta = \frac{2RTC_oN}{nF\pi^{1/2}}$$

Then some time τ is determined at which

$$\eta_\tau = \frac{RT}{nF}\frac{i}{i_o} \qquad (7)$$

that is, at which the concentration term is equal to the term related to the charging of the double layer

$$\frac{2N\tau^{1/2}}{\pi^{1/2}} = \frac{RTN^2}{nF} C_d$$

Thus, it follows that

$$\tau^{1/2} = \frac{RT}{nF}\frac{\pi^{1/2}}{2} N C_d = \frac{\pi}{4}\frac{C_d}{i}\delta$$

It is evident from this expression, that in order to find $J^{1/2}$ the double layer capacity (which may be determined by some other method) must be known. Knowing $J^{1/2}$ and using the graph $\eta - t^{1/2}$, we can find η_J and the exchange current, equation (7). Finally, by knowing i_o for different C^* at constant C_R^*, the values of k° and α can be determined by the previously described method.

2. Cyclic Galvanostatic Method: Wijmen and Smit[5] proposed a modification of the galvanostatic method. In this case, square wave galvanostatic pulses of a given frequency are applied to the cell and the shift of potential from equilibrium value is measured. (Figure 4)

The solution of Fick's diffusion equation in this case is more complicated than in the case of the basic galvanostatic method and can be obtained only by neglecting the effects of charging current. Therefore, this method is only applicable when the charging of the double layer is negligible. The cyclic galvanostatic method does not show important advantages over the basic current step method and consequently, it will not be described in more detail.

3. Double Pulse Galvanostatic Method: The galvanostatic method is limited because the charging current predominates for a very short time after the current step. As noted above, the equation derived by Berzins and Delahay[4] is valid only for $\tau > 7 \times 10^{-5}$ seconds. Gerischer and Krause[6] developed a double pulse method, which is described below. Two current pulses are applied consecutively to the electrode; the first, larger pulse, is expected to charge the electrical double layer to the over-voltage corresponding to the current density of the second pulse. The dependance

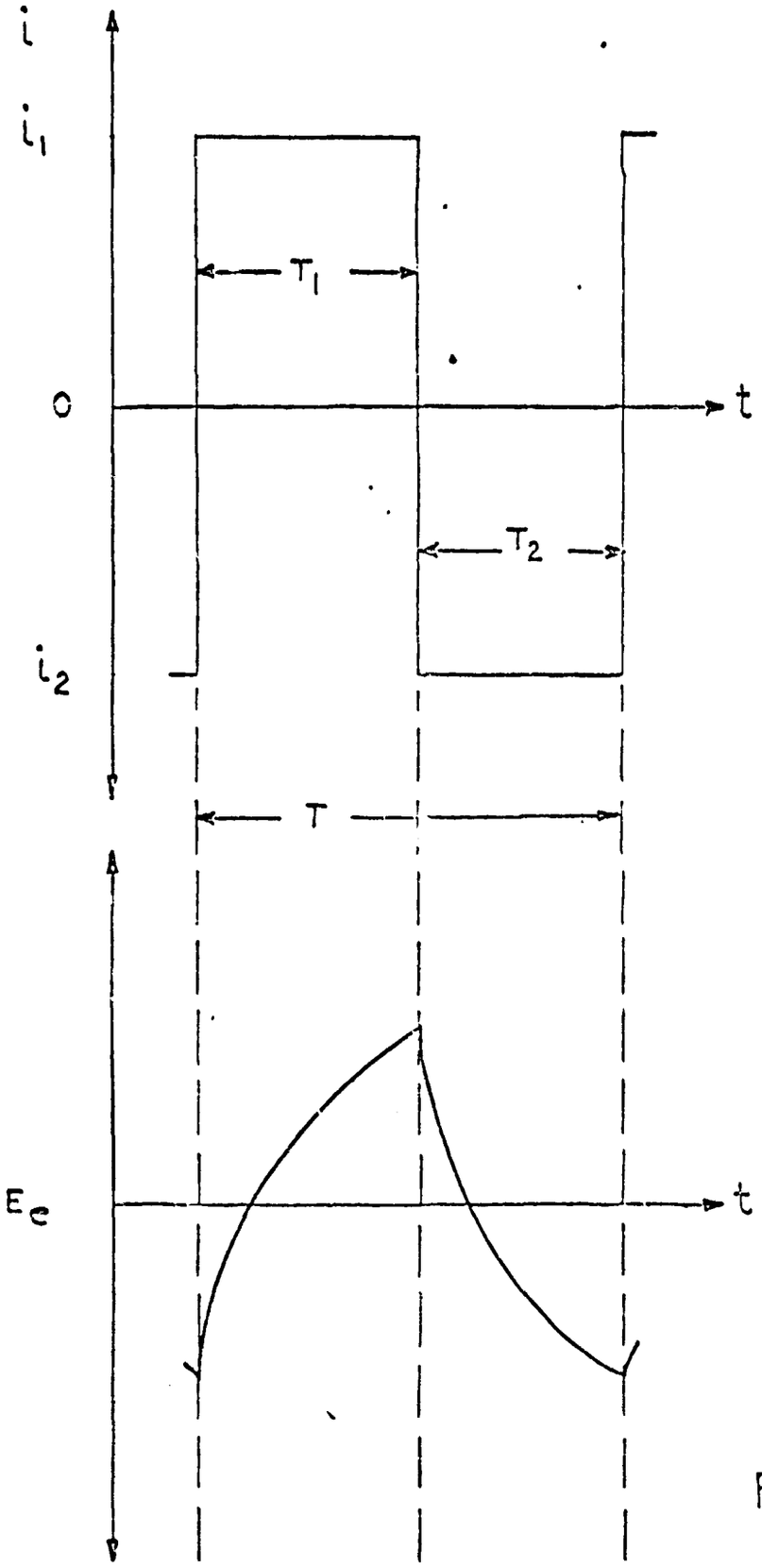

FIGURE 4

CYCLIC GALVANOSTATIC METHOD

of current on time and in the double pulse method is shown in Figure 5. The duration of the first pulse is approximately 1 μsec and the duration of of the second one approximately 10 μsec. If the ratio of the pulse is chosen correctly, that is, if the first pulse charges the double layer exactly to the over-voltage corresponding to the current density of the second pulse, a horizontal section should be observed at time t_1 corresponding to the end of the first pulse. Figure 6, illustrates the three possible cases: In curve 1 the double layer is over-charged and η decreases initially after the end of the first pulse (t_1); curve 2 corresponds to the correct ratio, and curve 3 shows that the double layer is not yet completely charged and η continues to increase after t_1.

Gerischer and Krause[6] assumed that the effect of concentration polarization can be neglected at the end of the first pulse. Then the quantity η_H corresponding to the initial section on the curve $\eta - t$ is related to the exchange current by a very simple relationship.

$$\eta_H = \frac{RT}{nF} \cdot \frac{i_2}{i_0}$$

Thus, the calculation of i_o and the kinetics parameters α and k° is relatively simple.

However, Matsuda, Oka and Delahay[7] showed that the assumption of Gerischer and Krause that the concentration polarization may be neglected at t_1 was incorrect. From the mathematical analysis of the dependance of η on t, at $\eta \ll RT/nF$ and small values of t_1, they obtained

$$\eta_H \cong \frac{RT}{nF} \cdot i_2 \left(\frac{1}{i_0} + \frac{2N}{3\pi^{1/2}} \cdot t_1^{1/2} \right)$$

that is, for sufficiently small values of t_1, the plotting of $\eta_H - t^{1/2}$, is a straight line with an intercept at $t_1 = 0$ equal to $(RT/nF)\frac{i_2}{i_0}$

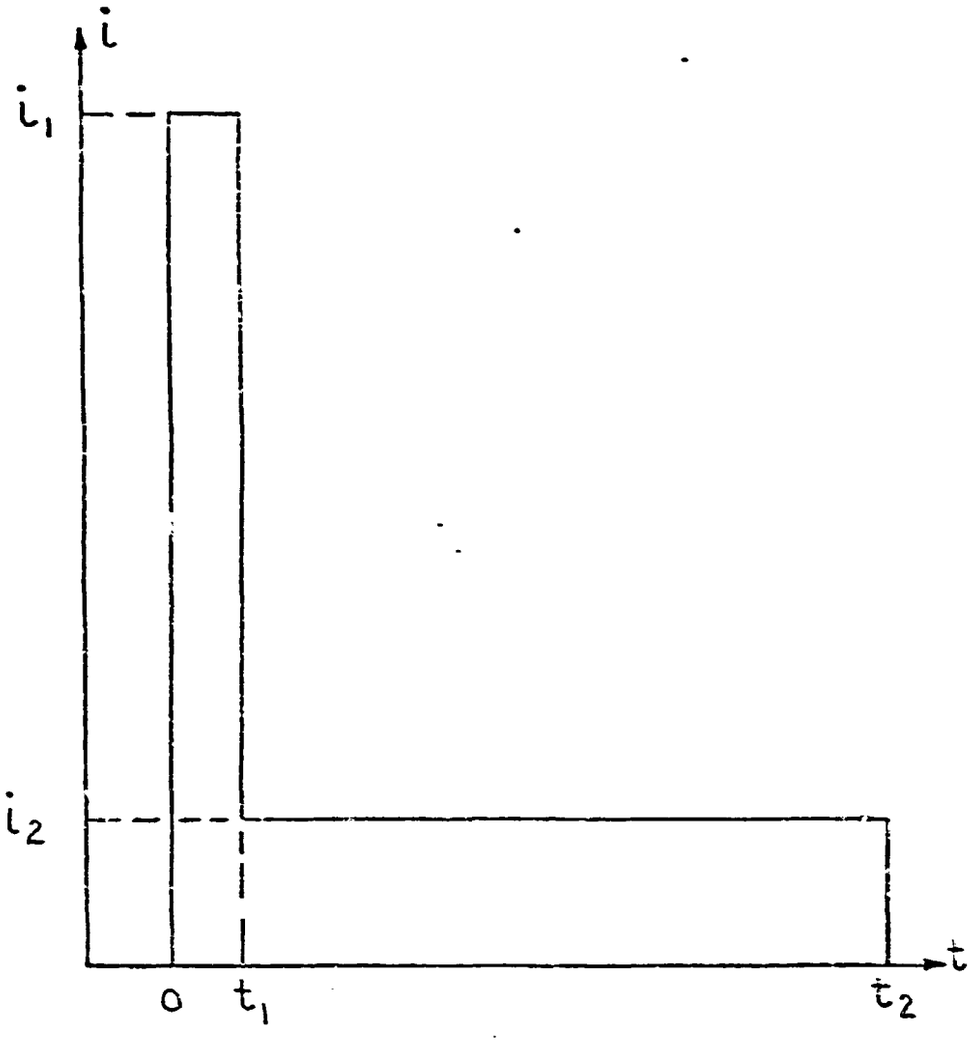

FIGURE 5

DOUBLE PULSE GALVANOSTATIC METHOD

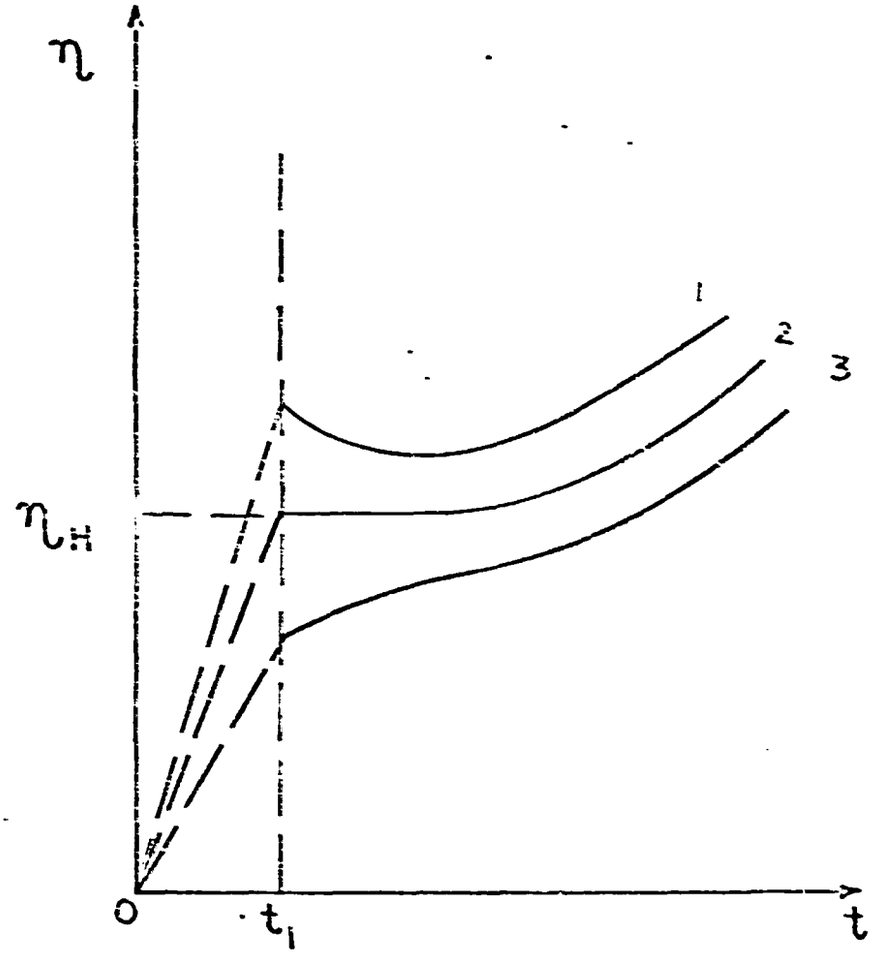

FIGURE 6

OVERPOTENTIAL TIME RESPONSE IN DOUBLE PULSE GALVANOSTATIC METHOD

This value can be quite different to the value of η_H at t_1.

c) COULOSTATIC METHODS

The coulostatic method was developed by Delahay and Aramata[8].

In this method, the charge density on the electrode, which is previously at the equilibrium potential E_e, is suddenly changed by some specific value. The circuit must remain open during this operation. In this case, the electrode potential changes sharply with respect to E_e as a result of the charge increment ΔQ ; then, as the electrochemical reaction proceeds, the potential gradually approaches its equilibrium value. Thus, in the coulostatic method, the variation of η with time is measured after some definite change has been applied to the electrode; the parameters of the electrochemical reaction k° and α are calculated from the η -t curves. The dependance of η on t was analyzed by Delahay and Aramata[8]. Assuming that

$$\frac{-i_o nF}{RT C_d i_o} \gg N^2$$

the relationship becomes

$$\eta \cong \eta_{t=0} \exp\left(-\frac{i_o nF}{C_d RT} \cdot t\right)$$

that is, η decreases exponentially with time.

Thus, the graph $\log|\eta|$ — t should yield a straight line, the intercept at t=0 determines $\eta_{t=0}$ which is directly related with the double layer capacitance by

$$C_d = \frac{\Delta Q}{\eta_{t=0}}$$

The slope of the line, equal to $i_o nF/2.3 C_d RT$ can be used to calculate i_o. The determination of both α and k° follows the same procedure described before; determination of i_o for different values of C°, at C_R° = const.

In comparing the coulostatic method with other relaxation methods, one should point out that this technique required the simplest experimental apparatus. The same concept of the coulostatic method was employed by Anson[9] in the development of the technique called Charge-step Chronocoulometry. In this case, the potential-time transient is converted in the corresponding charge-time transient by means of appropriate charge-potential data. The equation which relates charge-time behavior is

$$Q = Q^{\circ} + Q_{inj} - 2 n_1 F A C_o^{\circ} \left(\frac{D_o t}{\pi}\right)^{1/2}$$

where Q° is the initial charge on the electrode and Q_{inj} the charge injected. A plot of $Q-Q^{\circ}$ versus $t^{1/2}$ is linear with an intercept at t=0 corresponding to the injected charge. This method is attractive in the determination of reactant adsorption. The Q-t equation becomes

$$Q - Q^{\circ} = Q_{inj} - 2 n_1 F A C_o^{\circ} \left(\frac{D_o t}{\pi}\right)^{1/2} - n_1 F \Gamma'$$

where Γ' is the amount of adsorbed reactant in moles/cm^3. In this case, the difference between the intercept and the amount of injected charge, gives the amount of reactant absorbed.

d) ELECTRODE IMPEDANCE METHODS

The electrode impedance methods were initially developed by Randles[10], Gerischer[11], and Grahame[12]. A sinusoidal voltage of sufficiently small amplitude (few millivolts) was applied to the electrode, which was at the equilibrium potential. A.C. impedance bridges permitted the evaluation of the electrode reaction components by electrically equivalent analog circuits. These techniques will not be described in detail here; instead, an intro-

ductory explanation of a recent advance in impendance measurements which may have very wide application, is included. The study of the electrode process may be carried out by interpretation of relaxation data in the complex frequency domain corresponding to the Laplace variable, s [13]. The differential equations which describe the pulse effects on an electrochemical system can be solved by the application of the Laplace Transformation[14]. This method results in an algebraic equation, which is therefore simpler in form. As one example, let us consider an electrode process consisting of only linear diffusion and electron transfer, in which a constant current pulse is applied. Then, the total current I_T is the sum of the faradaic current I_F and the double layer charging current I_c. The Laplace Transformation of this statement is $I_T(s) = I_F(s) + I_C(s)$

By definition of capacitance charging current, $I_c(s)$ can be expressed by $I_C(s) = V(s)\, C_d(s)$ where V(s) is the overpotential developed across the double layer C_d during the pulse. In a same fashion I_F is given by [15]

$$I_F(s) = i_o\left[\frac{C_o(o,s)}{C_o^*} - \frac{C_R(o,s)}{C_R^*} - \frac{nF}{RT}V(s)\right] \quad (8)$$

Where Co (o,s) and C_R (o,s) are the transforms of the variations in time of the surface concentrations of O and R. The concentration ratios expressed in (8) are obtained by solving Fick's second law, considering semi-infinite planar diffusion. The solution yields an explicit expression for the faradaic current which may be written as

$$I_F(s) = \frac{V(s)}{B\sqrt{s} + nF/RT\, i_o} \quad (9)$$

where

$$B = \frac{RT}{n^2F^2}\left[\frac{1}{C_o^*\sqrt{D_o}} + \frac{1}{C_R^*\sqrt{D_R}}\right]$$

If we consider the total current constant, then $I_t(s) = I_T/s$ and the total expression becomes:

$$\frac{I_T}{s} = V(s)\left[\frac{1}{B\sqrt{s} + nF/RT\, i_o} + C_d s\right] \quad (10)$$

Inverse transformation of this equation for V(s) results in the well known expression for dependance of overpotential with time, equation (6) in the galvanostatic method. However, inspection of (10) shows that this equation contains all the kinetics parameters required for an electrochemical study, if direct use of the equation could be made. Analysis of Laplace Transformation shows that this is possible. Thus,

$$F(s) = \int_0^\infty f(t) \exp(-st)\, dt \qquad (11)$$

where $f(t)$ is the time domain function and s is the Laplace transform variable, which is a complex number, having a real, σ , and an imaginary, $j\omega$, part. This intergral exists only when $s = \sigma$ and $\sigma > 0$ for any time function which converges when multiplied by exp $(-\sigma t)$. This is true for practically all time functions of interest in electrode kinetics. When equation (11) is solved for $s = \sigma$, the result is termed the real axis Laplace transformation. It may also be performed, under certain conditions for $s=j\omega$ in which case the imaginary axis Laplace Transformation (Fourier Transformation) is effected. For this case (11) becomes

$$F(j\omega) = \int_0^\infty f(t) \exp(-j\omega)\, dt \qquad (12)$$

Imaginary axis transformation results in a complex function and consequently it has real, Re, and imaginary, Im, parts. It allows description of three basic functions: $Re(F(\omega)$, $Im(F(\omega)$ and $\theta(\omega)$, the latter being the phase angles normally defined for a complex number. The principal advantage of the transformation technique just described, is that, provided the system behaves in a linear manner, the impedance may be determined. Thus, functions $Z(\sigma)$ and $Z(j\omega)$ may be studied. Fortunately, these functions are simpler in form and therefore easier to interpret. In addition, as the transformation is done from t = o, results may be obtained along the rise of the pulse employed and since impedance is a characteristic only of the

system under study, the instrumentation effects may be eliminated. To give an example of the application of (11) and (12) let us consider an electrochemical system represented by the following circuit:

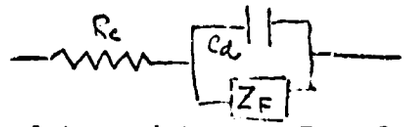

Where Re = electrolyte resistance; Z_F = faradaic impedance and Cd = double layer capacity. The expression for the transform of the total electrode impedance Z(s), may be written as:

$$Z(s) = Re + \frac{1}{1/Z_{F(s)} + Cds}$$

Inspection of (13) indicates that values of either σ or $j\omega$ may be used so that $1/Z_{F(s)} \ll Cds$, which, under practical conditions, means measurements at very short times. Thus, for $s \to \infty$, (13) becomes

$$Z(s) = Re + \frac{1}{Cds}$$

Now Re and Cd may be obtained in terms of σ and $j\omega$ using the appropriate integration. When these components are known, they may be subtracted from the total electrode impedance leaving the faradaic impedance for analysis. For the system under study and using (9) we have

$$Z_F(s) = B/\sqrt{s} + nF/RTi_o$$

which now may be analysed in terms of σ and $j\omega$.

Summarizing, the use of both real and imaginary axis transformations permit the interpretation of pulse data in a manner analogous to the way classical A.C. data is analysed[16, 17]. Because it is possible to obtain transformations along the rise of both the input perturbation and the response function, the electrode impedance can be obtained for frequencies at least three orders of magnitude higher than those readily obtainable using A.C. bridge methods, since measurements may be made at times down to 1 nanosecond. The data transformation technique may be applied to the pulse response of an electro-

chemical system without a prior assumption about the mechanism present. Once the transformation has been obtained, diagnostic criteria related mainly to the determination of number of time constants and their placement in the appropriate equivalent circuit for the impedance may be employed.

e) DECAY METHODS

The study of decay techniques have had less attention than the typical pulse methods. It is possible to study electrode decays from any of the three possible perturbations of the electrode: current, potential or charge step. For the charge step, we have exactly the case discussed before, known as the coulostatic method. Generally, decay studies follow the open circuit relaxation behavior of overpotential versus time so that conclusions obtained in the coulostatic method are directly included in any decay method.

The voltage decay at open circuit may be explained, to a first approximation, as the discharge of the double layer through the faradaic impedance. But there may be other effects which are apparently not connected with the capacitance. When electron transfer has occurred, there are concentration differences in the vicinity of each electrode. One may expect that, for a short time, a pulsed redox system could act as a concentration cell due to these differences. The decay voltage would be due to an electron transfer process. Obvious changes in the decay time response can be evoked by controlling the pulse width and amplitude of the perturbation. The time domain yielding the most pertinent data can thus be clearly specified. However, the

effects are also interrelated and very often they are not clearly separated. The classical straight line of the plot of log η vs. time is not always obtained. Piggin[18] has shown graphs with different slopes, altered by charge, pulse current and pulse length.

Decay studies should be oriented toward the control of the pulse used for the perturbation of the system to affect different parts of the equivalent circuit. If we consider again the case discussed in impedance techniques, it is clear to see that one must find time domains at which $Z_F \ll Cd$ and be able to separate different components of the overall equivalent circuit. It might be possible to improve the interpretation of η -t decay results using transformation techniques.

a) Ring-Disc Electrode Circuits

Two circuits were developed for the simultaneous control of two independent working electrodes and the consequent application to rotating ring-disc electrode techniques. The first one is shown in Figure 7. Since it is not possible to operate two independent electrodes connected to the same ground (i.e. the ring and the disc) at different potentials with respect to a reference electrode, the potentiostats were operated in the reverse mode. In this, a large platinum gauze electrode was used as a common counter electrode for both the ring and the disc and this was connected to 'ground'. This electrode was polarized cathodically from a second platinum gauze electrode (not shown) to the point of hydrogen evolution and under these conditions maintained a relatively stable potential ($\pm$5m V) as current was passed through it to the ring and the disc. The ring and the disc were connected to the control terminals of separate potentiostats operated in the follower mode and could be held at different fixed potentials or scanned independently with respect to the platinum gauze electrode held at 'ground' potential.

The second circuit is shown in Figure 8. Here, the ring and the disc are connected to separate ground points. This is achieved by controlling one of the electrodes in the conventional way with a Tacussel potentiostat and the other one by using one operational amplifier in the configuration shown in the figure but powered with batteries.

b) IR Compensation

FIGURE 7. RING-DISC ELECTRODE CIRCUIT - Nº I

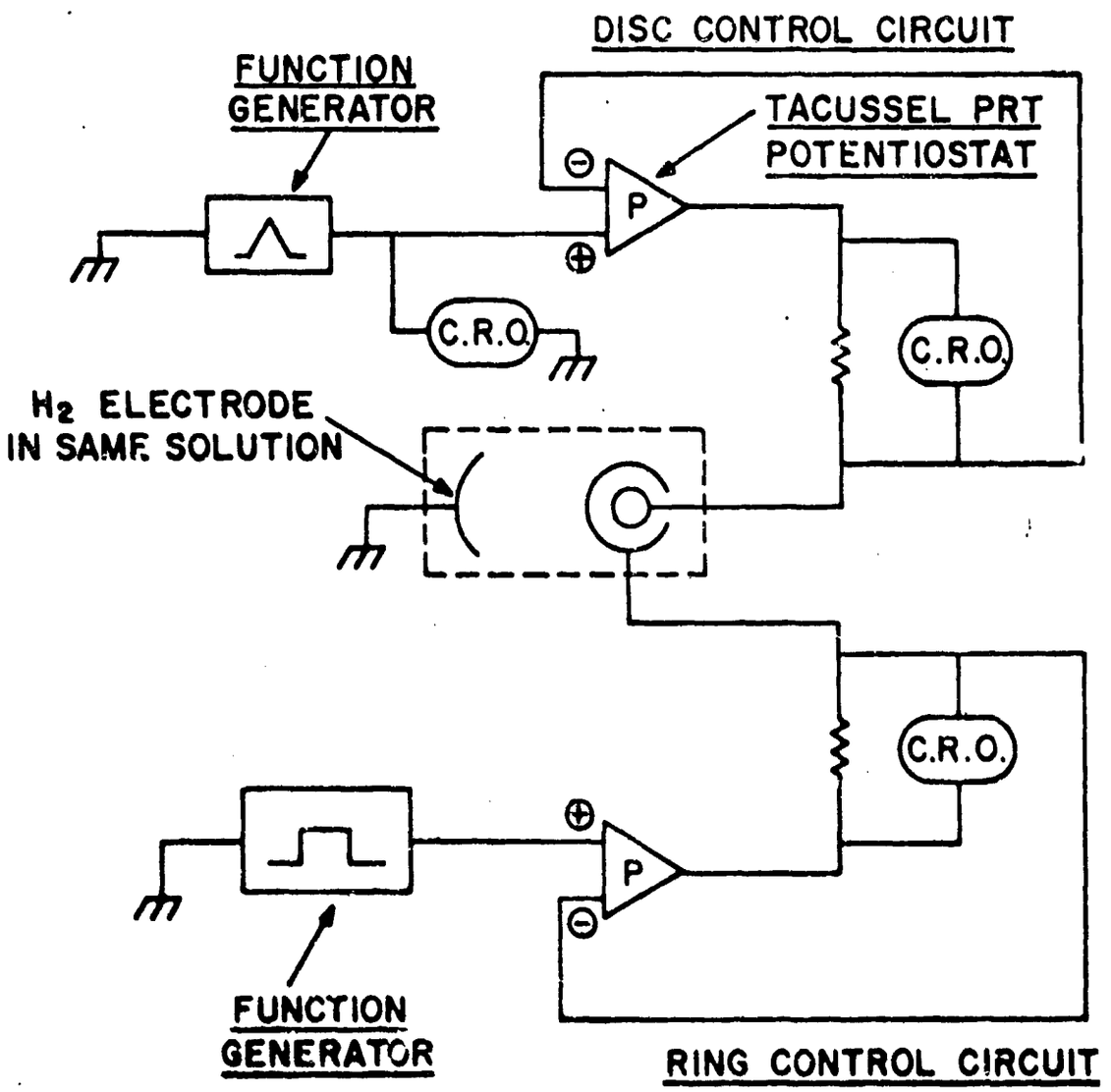

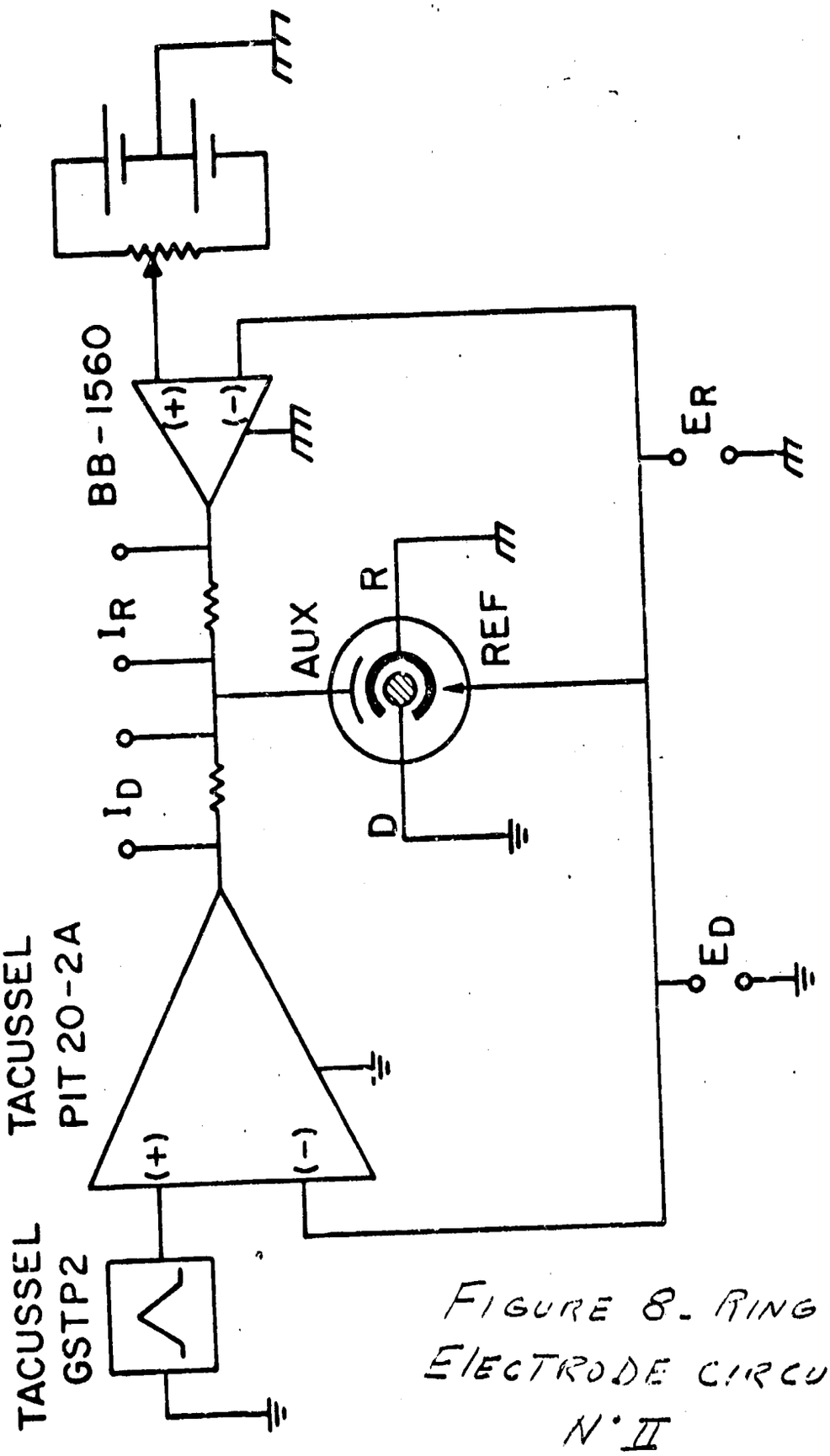

FIGURE 8. RING-DISC ELECTRODE CIRCUIT. N° II

Figure 9 shows the configuration of our potentiostatic system plus the inclusion of the IR compensation obtained by positive feed-back. The use of operational amplifiers of the type of G&I 9186 permitted very fast IR compensation, eliminating up to 95% of the IR drop.

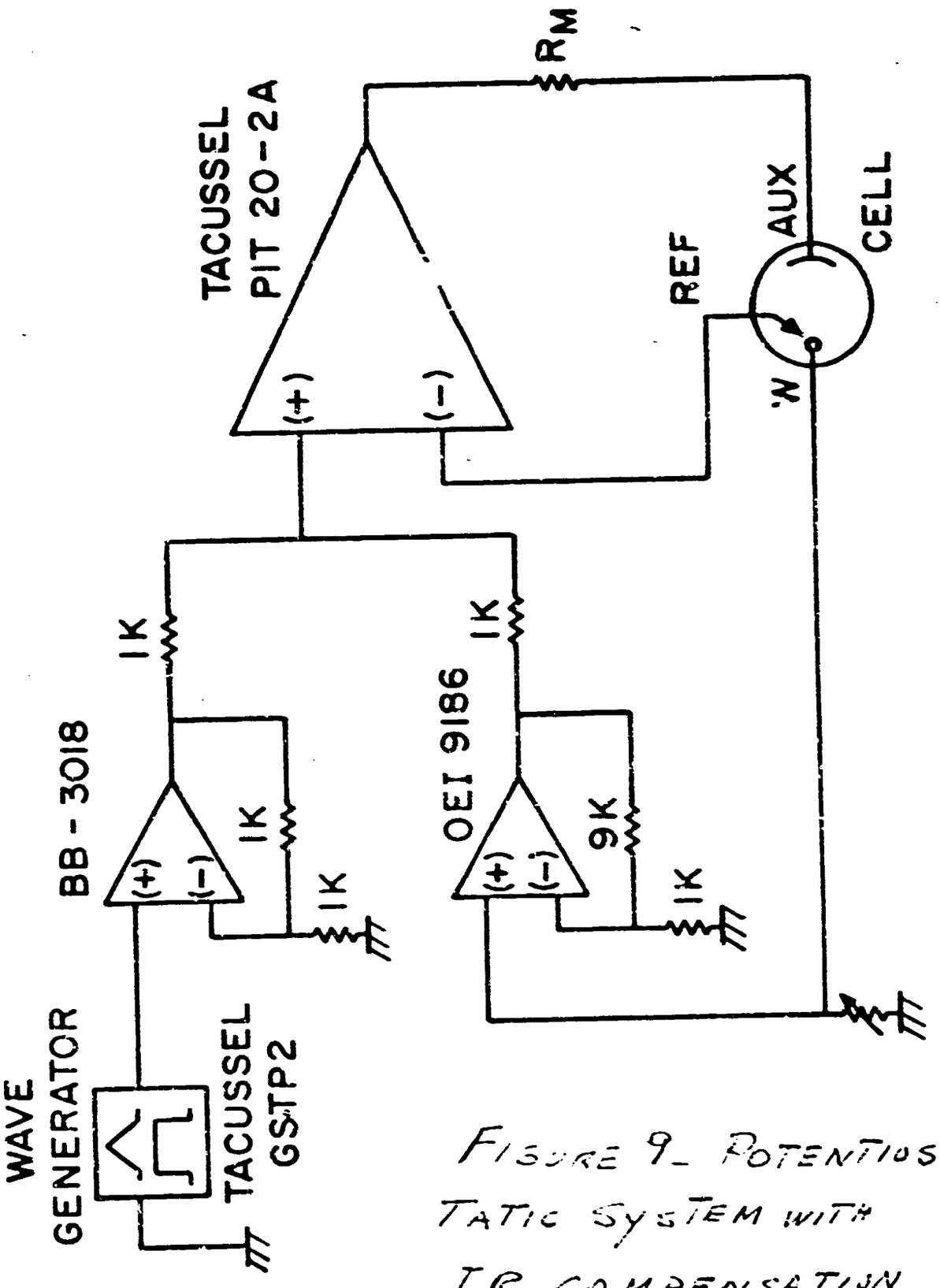

FIGURE 9_ POTENTIOSTATIC SYSTEM WITH IR COMPENSATION.

C CHARACTERIZATION OF MERCURY BATTERIES BY PULSE TECHNIQUES

Basic research has been done on the electrochemical characterization of Mercury batteries by pulse techniques. From a fundamental research point of view, the studies should include an independent analysis of the electrode processes of both battery electrodes; the anode, amalgamated zinc and the cathode, mercuric oxide (HgO). To accomplish these separate analyses, both electrodes must be referred to an isolated reference electrode. Due to the small volume of the cells, a special miniature reference electrode has been constructed, consisting of a metal wire covered with a film of the corresponding oxidized specie. Because the electrolyte is concentrated potassium hydroxide saturated with zinc oxide, we decided to test the couples $Zn/Zn(OH)_2$ and $Cd/Cd(OH)_2$ as reference electrodes. The stability of these chemical systems was tested using the classical method of small overpotentials (Tafel plot in the linear region) - Refer to Figure 10. The 0.1 millivolt resolution required for overpotential and current measurement was provided by a Systron Donner Model 1033 Digital Voltmeter with a high impedance Keithley Model 602 Electrometer-follower to eliminate electrode polarization. A Tacussel pocentiostat (PIT 20-2A) and function generator (GSTP2) were used to supply the overpotential. Zinc and cadmium wire electrodes covered by their hydroxides were tested in solutions similar to the battery electrolyte. Overpotentials, not larger than $\pm$10mV were applied to both sides of the equilibrium potentials. The steady state current was measured and plotted versus overpotential. Bipolar overpotentials were applied in an attempt to determine the existence of hysteresis.

In general, $Cd/Cd(OH)_2$ showed slightly better performance than $Zn/Zn(OH)_2$. Figure 11 shows the results of a test performed with $Cd/Cd(OH)_2$ at 25.0°C.

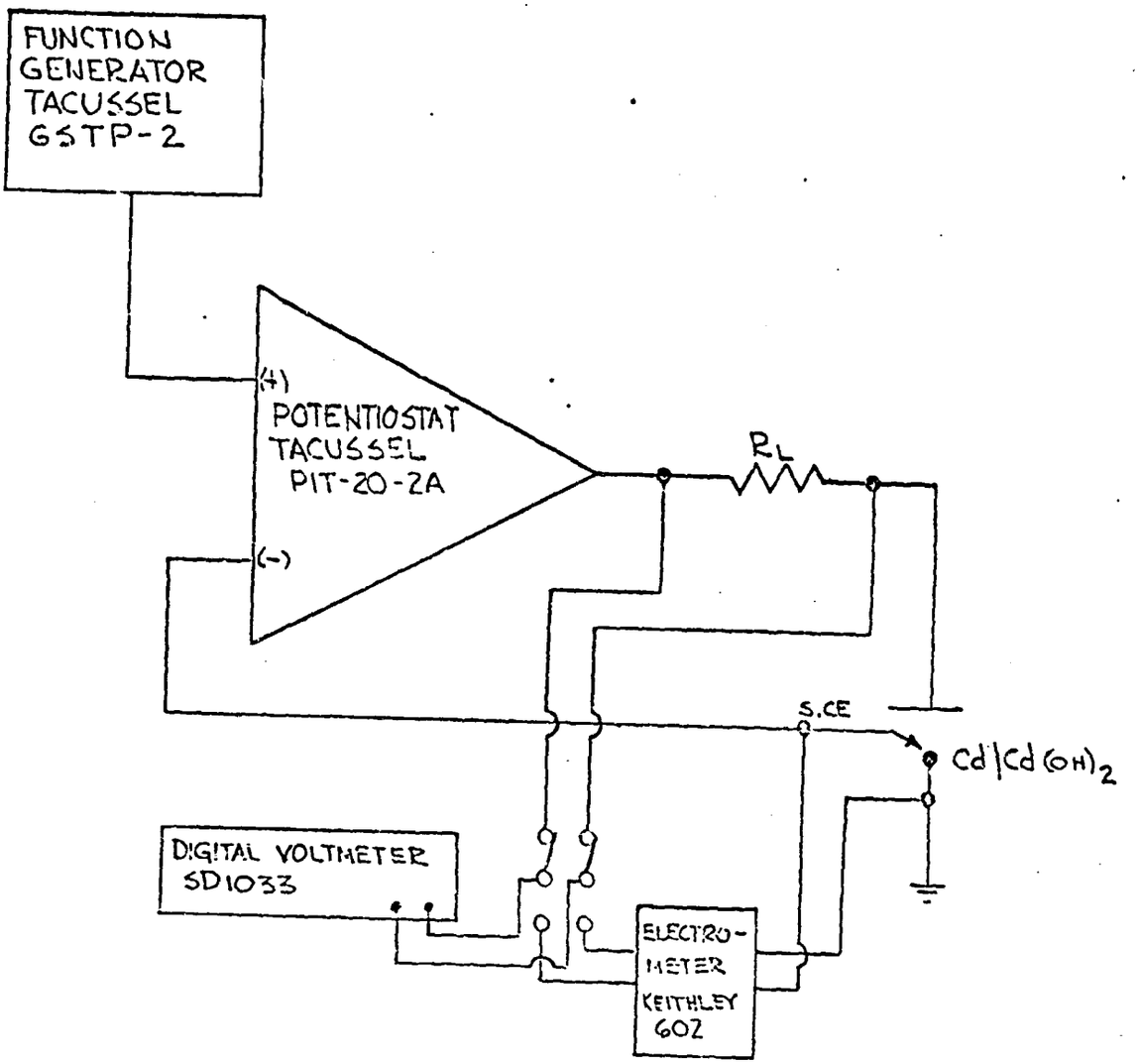

FIGURE 10

CIRCUIT DIAGRAM FOR REFERENCE ELECTRODE TESTING

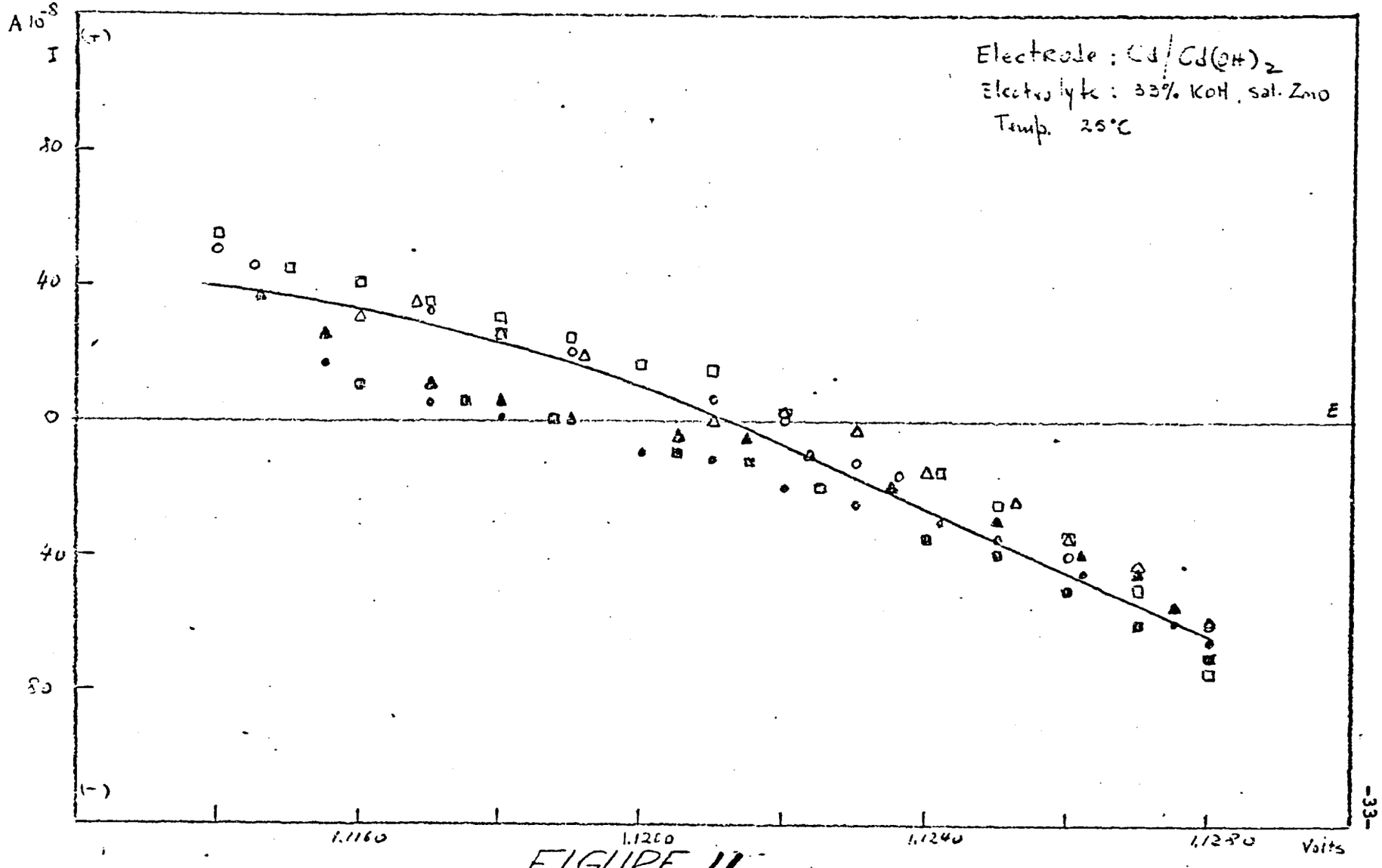

FIGURE II

BEHAVIOR OF THE Cd/Cd(OH)$_2$ ELECTRODE UNDER SMALL OVERPOTENTIALS

From the figure, the electrode potential is 1.121 ±0.0002 volts versus S.C.E. The $Cd/Cd(OH)_2$ reference electrode was employed in batteries of the type Burgess Hg 1R as is shown in Figure 12. A thin wall of Teflon tubing was used to protect against short circuits with the battery electrodes. The wire reference electrode was positioned just to the lower end of the Teflon tubing. This arrangement behaves very satisfactorily and has proven very useful for the simultaneous study of each electrode in relaxation studies. The circuit employed for the current pulse experiments is described in Figure 13. The square wave current pulse is obtained from a Data Royal Model F230A wave generator with the appropriate resistor. This resistor was also used for the current measurement. The overpotential time behavior of each electrode referred to $Cd/Cd(OH)_2$ was displayed on a dual beam oscilloscope (Tektronix, Type 556). The overpotentials were measured using the type W differential plug-ins on the "R" position to eliminate any possibility of loading the reference electrode. The current pulse was recorded simultaneously on a separate scope, using a Type 1A5 plug-in. The trigger from the first scope was used to initiate the second scope sweep and the pulse from the generator.

A large variety of tests were performed to identify the most efficacious experiments. Different current levels and pulse durations were the principal variables and their effect on overpotential-time curves, during the pulse and also during the decay period was observed. Both parts of the relaxation experiments were searched to identify the time domains yielding the most meaningful data. Some conclusions were reached, which may be useful for planning future experiments. If studies are concentrated in the pulse period, current level, and not duration of the pulse may be the

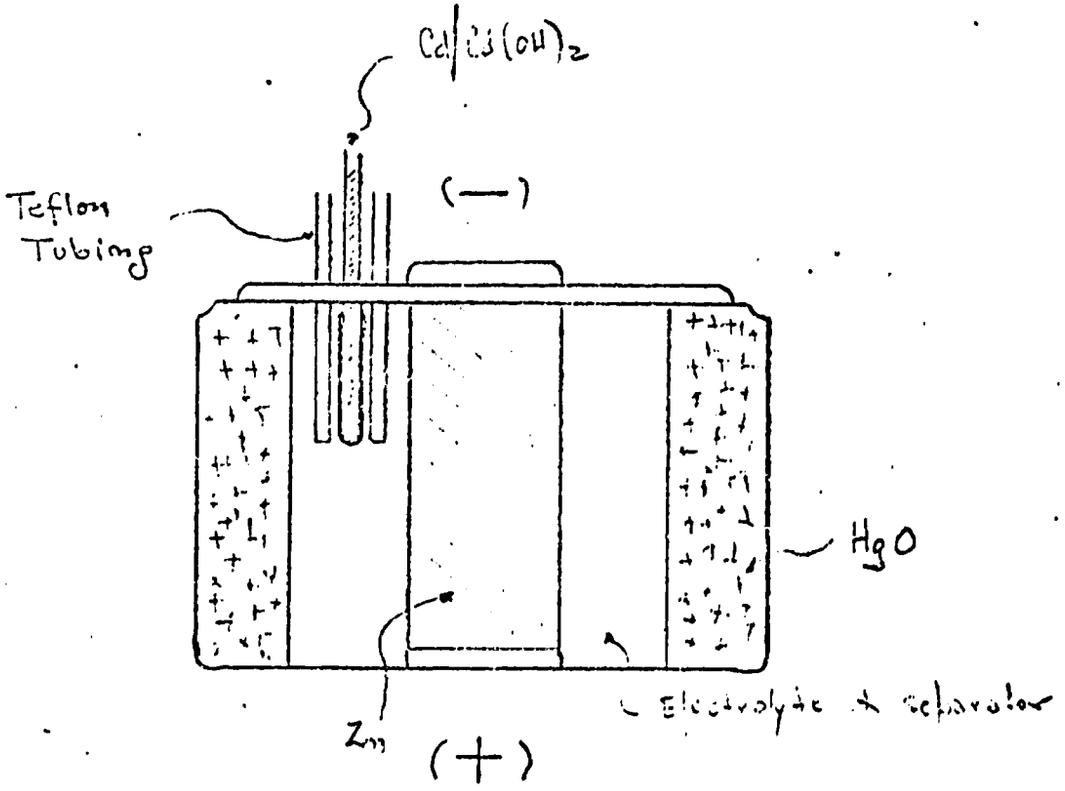

FIGURE 12
TYPICAL LOCATION OF THE REFERENCE ELECTRODES IN A MERCURY BATTERY

principal variable. Apparently, pulses in the order of milliseconds are long enough to permit the study of the principal features of the electrode mechanism. As expected, larger currents increase polarization effects. It is quite possible that the most valuable experiments may be those run at maximum current permitted without permanent deterioration of the battery. However, comparison of results at different current levels must be run to determine compatibility and optimum experimental conditions. Fast rise times are of great importance to provide useful data as close as possible to the initiation of the perturbation. The instrumentation described in Figure 13 yielded rise times on the order of 0.5 microseconds.

The following is a description of some of our experiments demonstrating the promise of pulse methods in battery characterization. Figure 14a and 14b show the overpotential-time response of each battery electrode during and after the galvanostatic pulse. Figure 14a corresponds to a new battery and Figure 14b to the same battery after 50% discharge. It is apparent from these figures that the behavior of each electrode is quite different. Polarization effects are more pronounced in mercuric oxide than in zinc. The overpotential of the positive electrode does not reach steady state, during the pulse (3 milliseconds), even in the case of the new battery. The overpotential-time plot for the zinc amalgamated anode is quite different. The overpotential has reached a constant value at approximately 1.5 milliseconds. The electrode resistance, as expressed in the initial IR drop, is different for each electrode. After the discharge, the resistance of the anode has decreased, while the mercuric oxide resistance shows minimal change. The effect on the anode might be explained by increase in mercury

concentration in the amalgam, because some zinc has been disolved in the electrolyte. We anticipated a drop in mercuric oxide resistance due to the formation of mercury metal in the reduction of the cathode. Apparently, other effects, requiring more research, combine to keep this electrode at almost the same resistance value. Figures 14a and 14b are only two experiments of a long series studying different time ranges in order to cover in detail all the changes of the overpotential versus time. Laplace transformation analysis was performed on the overpotential data and the driving current function to allow application of the aforementioned impedance techniques.

Figure 15 is a plot of $1/Z\ (\sigma)$ vs. σ for the zinc anode before and after the discharge. Analysis of the plot indicates a simple parallel RC circuit. To achieve this, we assumed an equivalent circuit of the following type:

and that Re is very small, as is the case in our battery (< 0.2 ohms). The total impedance may be expressed by

$$\frac{1}{Z(\sigma)} = \frac{1}{R_f} + C_d\sigma$$

If the plot yields a straight line, as occurs in the figure, the intercept should express the faradaic resistance and the slope gives the double layer capacity. From the plot, we observe that the double layer capacity did not change significantly during the discharge and it appears that the faradaic impedance has decreased after the discharge. These assumptions are very tentative and they are included here only to demonstrate the possibilities of the method. For example, it is quite unlikely that R_f for the case of the zinc oxidation, could be represented by only a simple

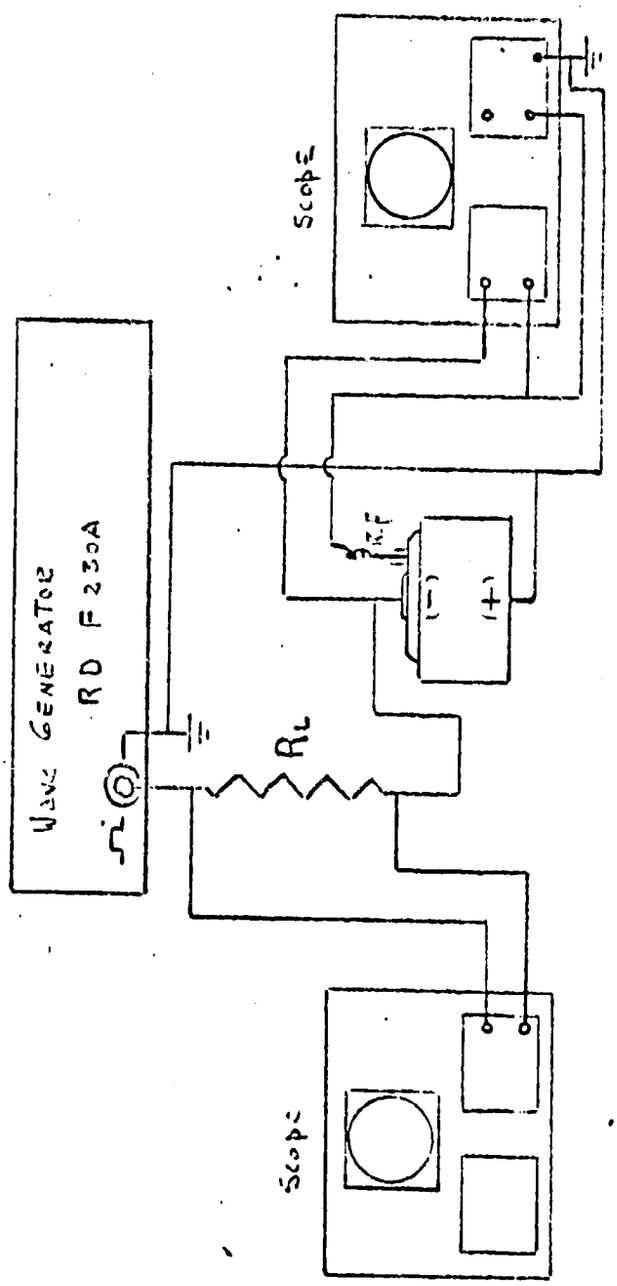

FIGURE 13

GALVANOSTATIC EXPERIMENT WITH MERCURY BATTERY

(Continued on Page 39)

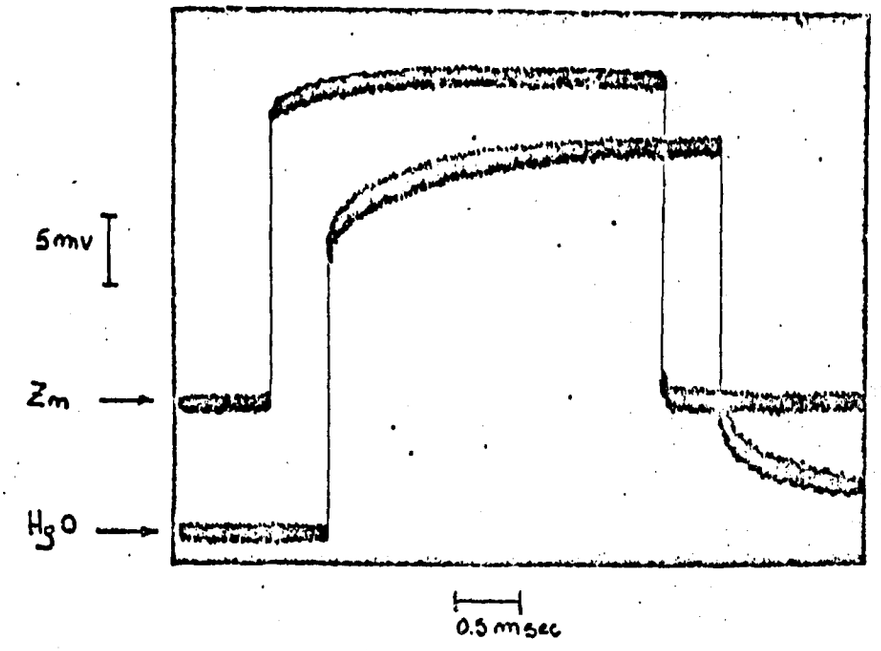

(a)

CURRENT · 50 ma

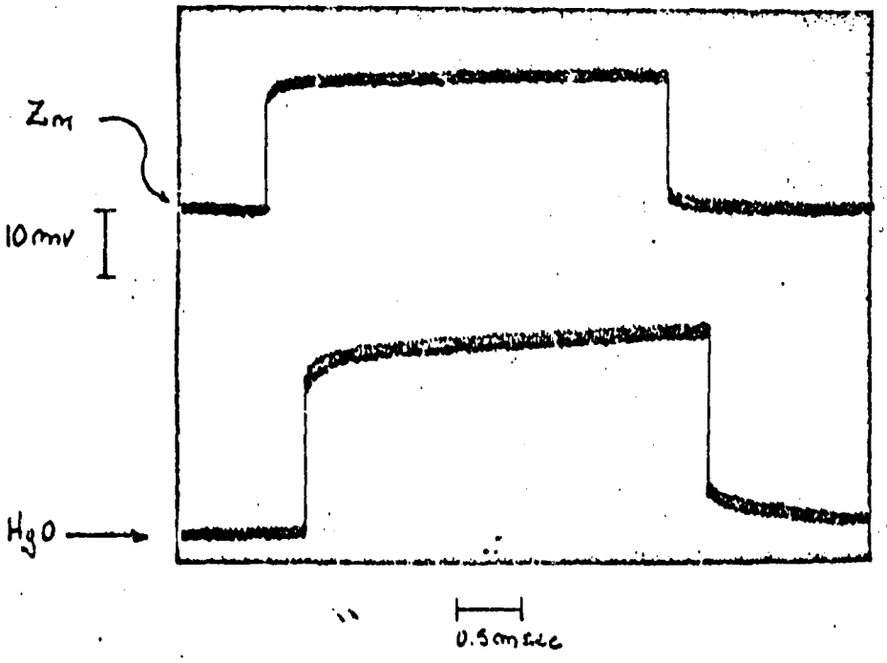

(b)

FIGURE 19
OVERPOTENTIAL TIME RESPONSE OF MERCURY BATTERY ELECTRODES

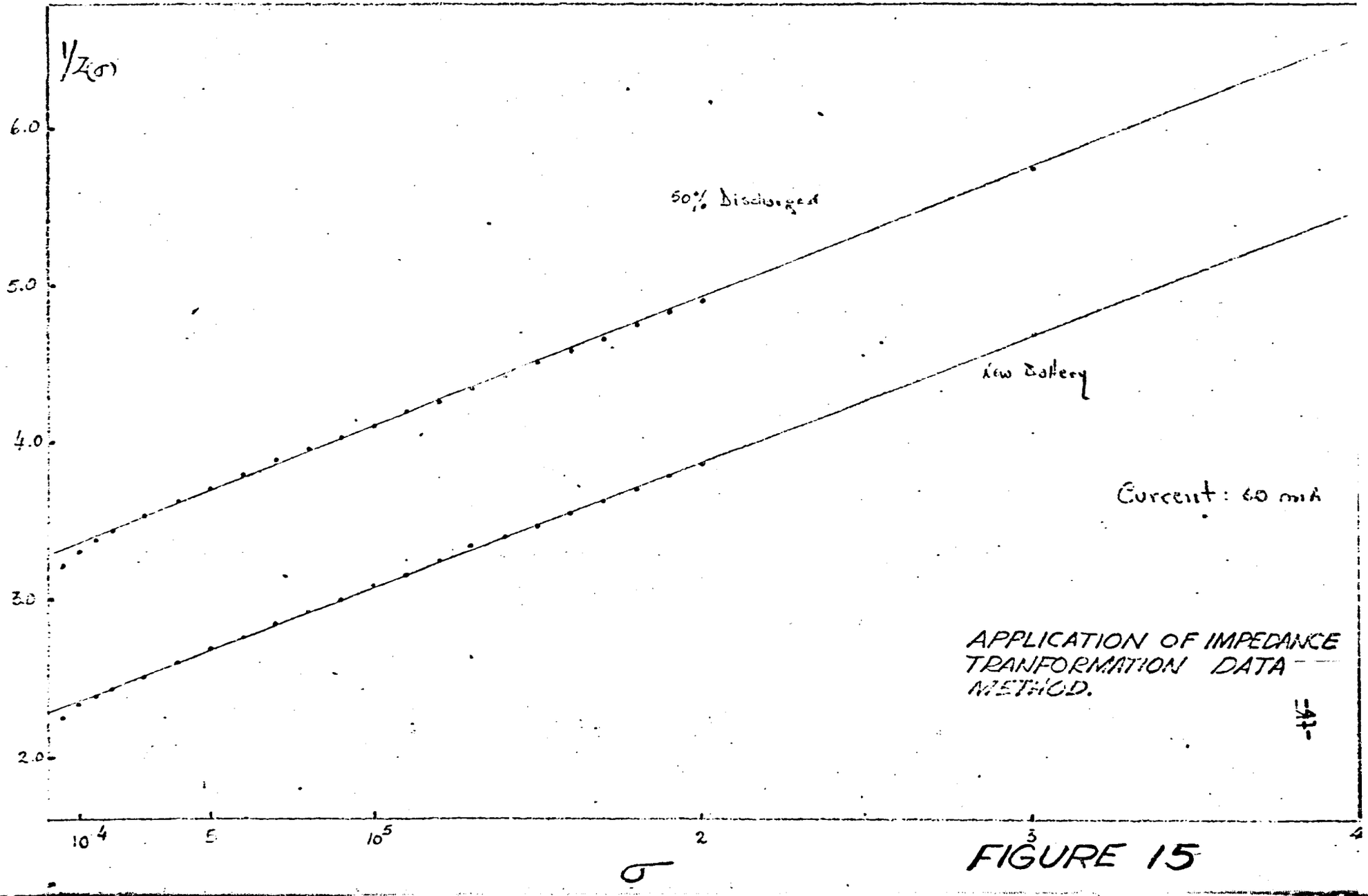
1/Z(σ)
6.0
5.0
4.0
3.0
2.0
50% Discharged
New Battery
Current: 60 mA
APPLICATION OF IMPEDANCE TRANFORMATION DATA METHOD.
-41-
10^4
5
10^5
2
3
4
σ

FIGURE 15

resistance. Ultimately, the representative circuit for R_f would have to be a complex R-C combination. Figures 14a and 14b also show the potential decay after the pulse. They show quite clearly that the zinc anode recovers much faster than the mercuric oxide. Figure 16 shows the results of a similar experiment on a battery which had been severely discharged. Here, the HgO recovery is very slow and shows how important this period (after the pulse) might be to the battery characterization. The zinc electrode shows an interesting overshoot which has been observed in several series. This special behavior may be related to the well known oxide formation on the electrode surface. We feel that these experimental results verify our original contention concerning the efficacy of simultaneous and independent study of both electrodes in the mercury cell. Indeed, Figure 16 shows very vividly how the different electrode mechanisms affect the electrode response to identical perturbations.

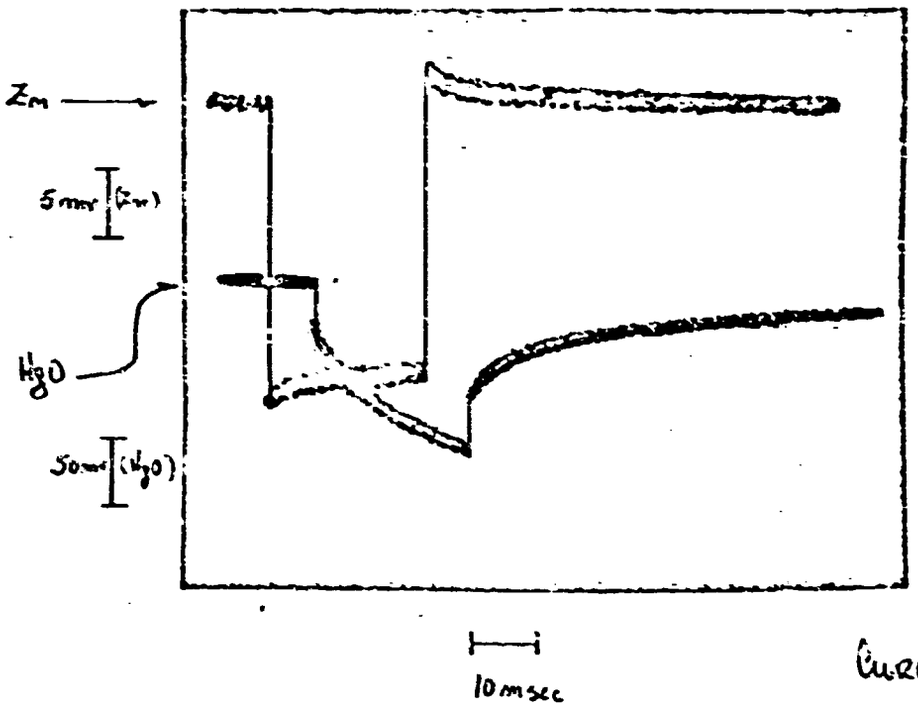

FIGURE 16

OVERPOTENTIAL TIME RESPONSE OF THE ELECTRODES OF A SEVERELY DISCHARGED MERCURY BATTERY

D THE ELECTROCHEMICAL REDUCTION OF m-DINITROBENZENE (m-DNB) IN MAGNESIUM PERCHLORATE SOLUTIONS

m-DNB is without any doubt, the organic cathode which has had major attention in the development of primary batteries. Several research studies[19,20,21] have intended the postulation of a mechanism for its reduction but, nevertheless, one must recognize that there is yet a quite wide research field open to more investigation. An electrode mechanism which may include as much as twelve (12) electrons transfers plus unavoidable coupled chemical reactions must have enormous mechanistic complications. In the present research work, we concentrated our study on the electrolyte formed of aqueous solutions of magnesium perchlorate, covering the pH range of 2 to 8. This upper limit was set up by the precipitation of magnesium hydroxide. In addition, we did our work only on the first two (2) reduction steps observed in this media. A third reduction process which appears only in a more restricted pH range and occurs at very negative potentials, very close to the decomposition of the electrolyte, was not studied.

Our principal objective was to postulate an overall mechanism for those two reductions steps and to do that we employed a series of modern electrochemical techniques and tried to interpret the results obtained by combination and comparison of their experimental data. The techniques applied were: Linear sweep voltammetry, in the single or the cyclic fashion, rotating disc electrode; potential step pulse and rotating ring-disc electrode.

Experimental

As the reduction of m-DNB consumes protons, the experimental results are not reliable if they are not performed under controlled conditions of pH. Thus, in all our experiments, the electrolyte was a solution of 0.5 M $Mg(ClO_4)_2$ plus the addition of a buffer which set the pH value. Different proportions of acetic-acetate were employed for the pH range 2 to 5 and the mixtures of borax-boric acid were used between 6 to 8. The concentration of these buffers was in the order of 0.1M or lower and the reliability of the buffer effect, in the complete electrolyte, was tested by appropriate titrations. The solutions with m-DNB had a concentration of 5 mM, a value very close to saturation in these medias. Two electrode-electrolyte systems were employed. At the beginning of our work, we used carbon-paste disc electrodes with a mixture of m-DNB and carbon, prepared in the conventional way, developed by Adams and co-workers[22]. The mixtures were in fact true m-DNB mixtures for battery plates. Later, during the principal part of the work, we employed pyrolytic graphite disc electrodes (PGE) in combination with buffered solutions of m-DNB. Carbon paste electrodes mixed with the electroactive material, in this case m-DNB, may provide an attractive approach to the electrochemical study of insoluble substances, and in addition they may simulate more closely the real electrode configuration of a battery. But the lack of theoretical study in the behavior/interpretation of results is very difficult and only qualitative information arises from the experiments.

Experimental Results

In Figure 17, we have two typical linear sweep voltammograms of m-DNB, at pH 6.1. The second curve shows the cyclic voltammogram of a carbon paste disc electrode of composition: m-DNB: 77%, carbon: 23% w/w; and the first curve is a cyclic voltammogram of a solution of m-DNB (3m M) using PGE as working electrode. In both cases one may observe two reduction steps, which are obtained at almost the same potentials (all potentials in this work are vs. S.C.E.). It is difficult to make comparisons because while in both cases the electrode active material is the same, the mass transport may be quite different. With the carbon paste electrode one may expect that the electrochemical reaction takes place within and at the surface of the m-DNB crystals, and the nature of the crystals and contact with the solution should have an effect in the process. Moreover one should consider that porous effects may participate and since we know that m-DNB is partially soluble, diffusion in the solution may occur. On the other hand, the system composed by PGE-m-DNB solution is a conventional case of an electroactive substance dissolved in an electrolyte and the mass transport must be diffusion controlled. We may add to the analysis of these curves, that there are no oxidation processes in the vicinity of the reduction steps, which would indicate that they consist of an irreversible mechanism. Another observation is the formation of a film on the electrode surfaces. After only one cycle run, both electrodes show effects of inactivation. Good reproducibility is obtained if the carbon paste electrode is refilled or if the PGE is rubbed on a smooth surface, such as a sheet of typing paper. The loss of activity required this type of pre-treatment before each run.

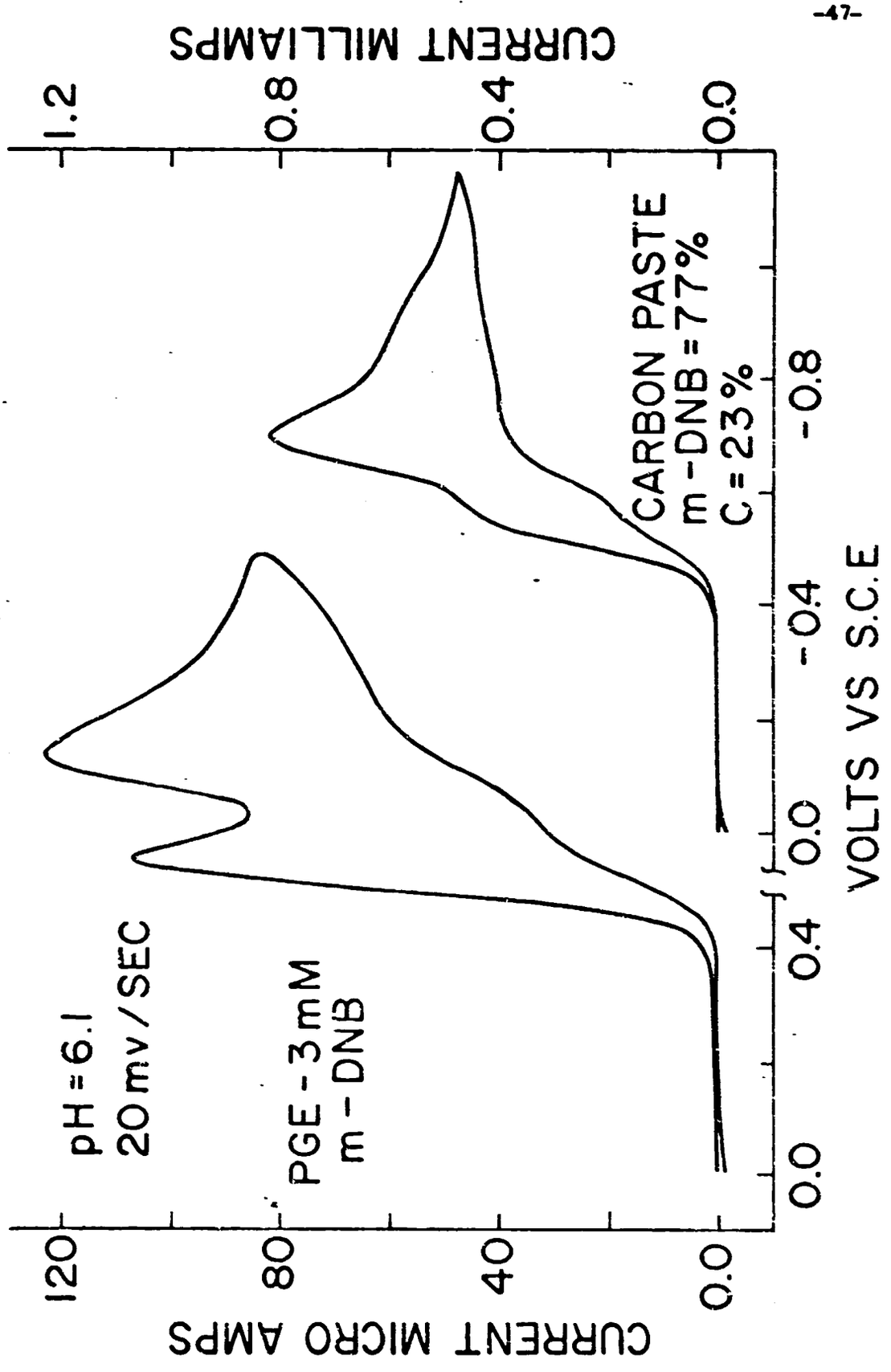

FIGURE 17- CYCLIC VOLTAMMOGRAMS OF m-DNB

Concentrating our study on the system formed by PGE and solutions of m-DNB, (Figure 18) shows other cyclic voltammogram, but in this case at a different pH, (3.9) and includes a very large range of potential. The voltammogram shows the three reduction processes, to which we referred before, and one anodic peak which appears at quite positive potentials relative to any of the reduction processes. This anodic peak is very broad and its current value very low. The third reduction peak was not studied and the anodic peak has some relation with the two first reduction steps, but this relationship is not very clear. For example, it is always obtained on reversing the potential after the first or second peak and the only difference observed is an increase in current. We are going to discuss this anodic process, in more detail, with the experimental results from rotating ring-disc electrode technique. The next,Figure 19,shows the effect of pH change on the characteristics of the two reduction steps. This figure has four representative voltammograms of m-DNB at pH 2.7, 4.7, 6.1 and 7.7. The effects observed are not very drastic and sometimes difficult to be analyzed. The general trend shown with pH increase may be summarized as follows: peak potentials shift to more negative values, (at least up to pH 6); the peak currents increase; there is a better separation between the reduction steps and finally it appears that the ratio Ip (II)/Ip(I) also increases. These pH effects are better defined between pH 2 to 6 but over 6, tc 7.7, the maximum pH tested, they are not very important and in some cases, such as peak potentials, the effect appears inverted.

The principal study uses cyclic voltammetry, and in order to determine the mechanism of an electrode process,must include the scan rate effect on the peak current. This type of study was done at different pH's and demonstrated

FIGURE 18. Cyclic VOLTAMMOGRAM of m-DNB – PGE.

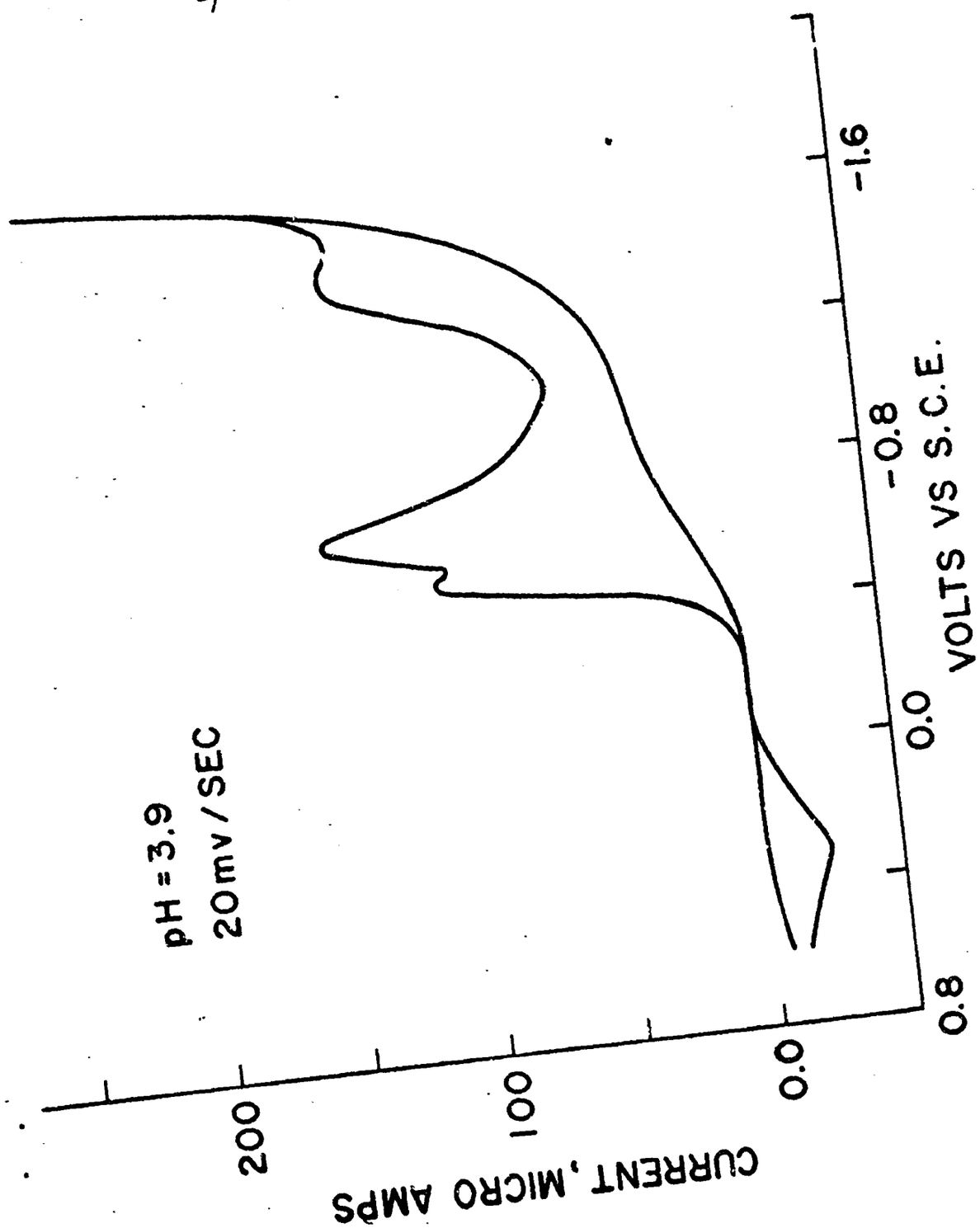

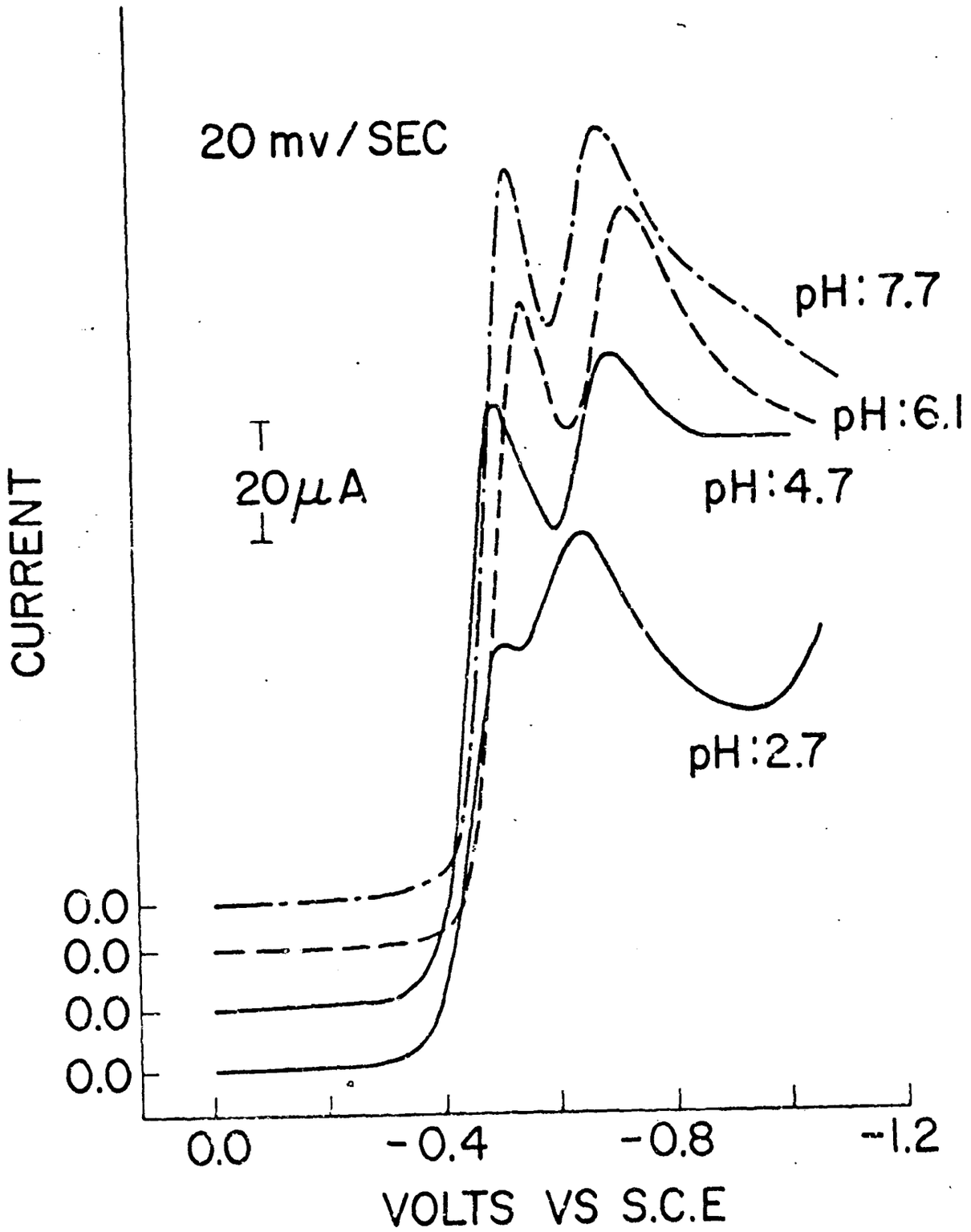

FIGURE 19. pH EFFECT

that the effects observed are practically the same in the whole pH range considered. Figure 20 shows several voltammograms which represent the behavior of the system under different sweep rates. They were run at pH 6.1. Observe how peak I increases, while peak II decreases, until it disappears with faster and faster scan rates. This figure shows quite clearly how peak potentials are shifted following the well known trend of irreversible electrode processes. These effects can be analyzed better by the conventional plot of $Ip/v^{\frac{1}{2}}$ vs v which is shown in Figure 21. The fact that both peaks give curves instead of straight lines, is an indication that both reduction steps have kinetic complications. These two plots demonstrate that we do not have the case of two consecutive electron transfers. This latter mechanism must give straight lines even for irreversible charge transfers. The curve which corresponds to peak II shows a very well defined trend and may be interpreted easily. The peak current of step II decreases sharply, vanishing to zero.

This behavior can be directly interpreted as a charge transfer with a preceding chemical reaction. Other cases which would also show a decrease of peak current, such as catalytic reactions or following chemical reactions will not vanish completely, as peak II does. If peak I would show a straight line, we would be able to diagnose an ECE mechanism (electron transfer-chemical reaction-electron transfer) with the second charge transfer occurring at more negative potentials than the first one, but from the figure we can see that our case is more complicated than that and step I is also affected by kinetics problems. A type of plotting as the one shown for peak I, with two distinctive plateaus at different scan rate ranges, and with the first one higher than the second one, is generally indicative

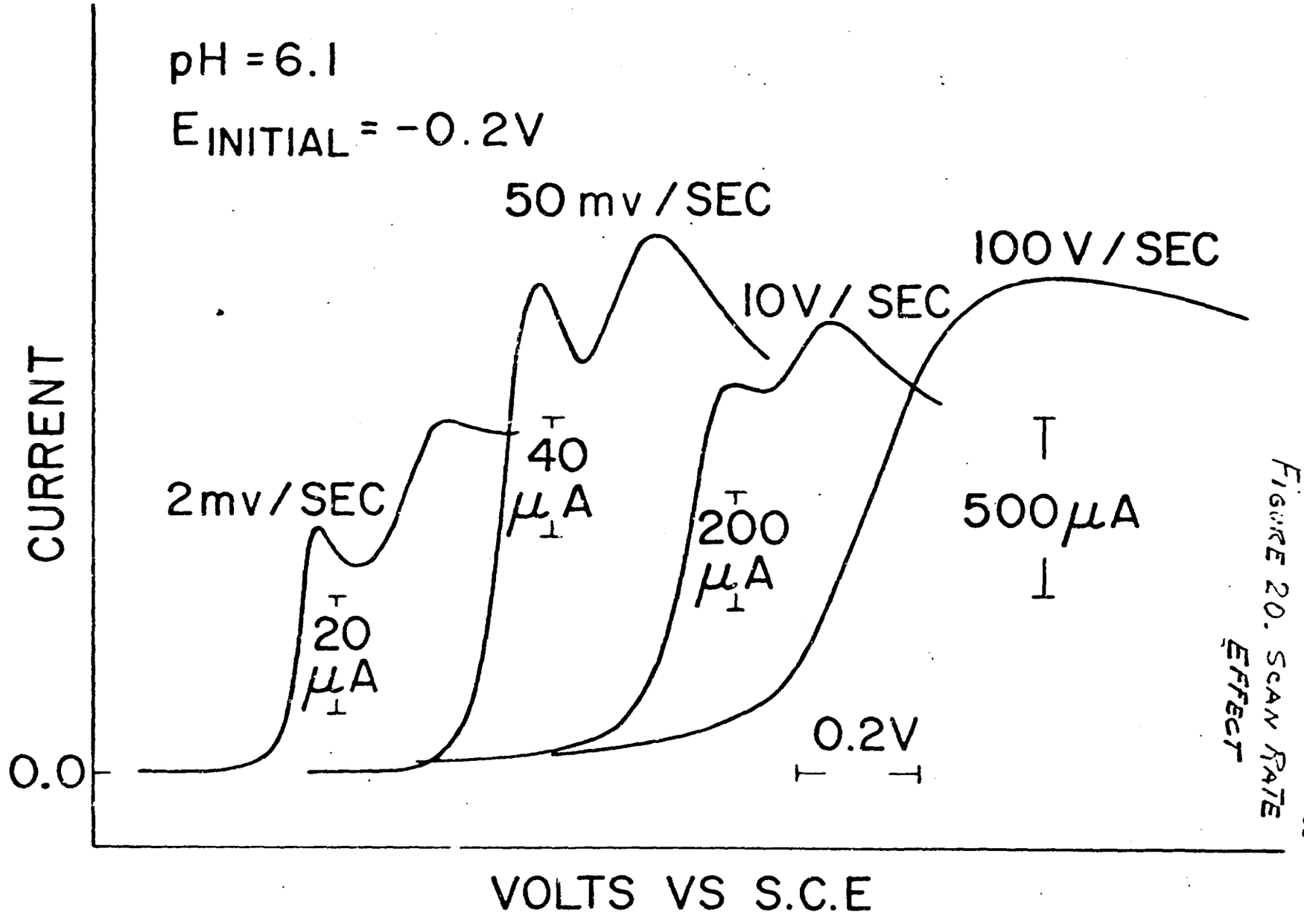

FIGURE 20. SCAN RATE EFFECT

FIGURE 21_ SCAN RATE EFFECT

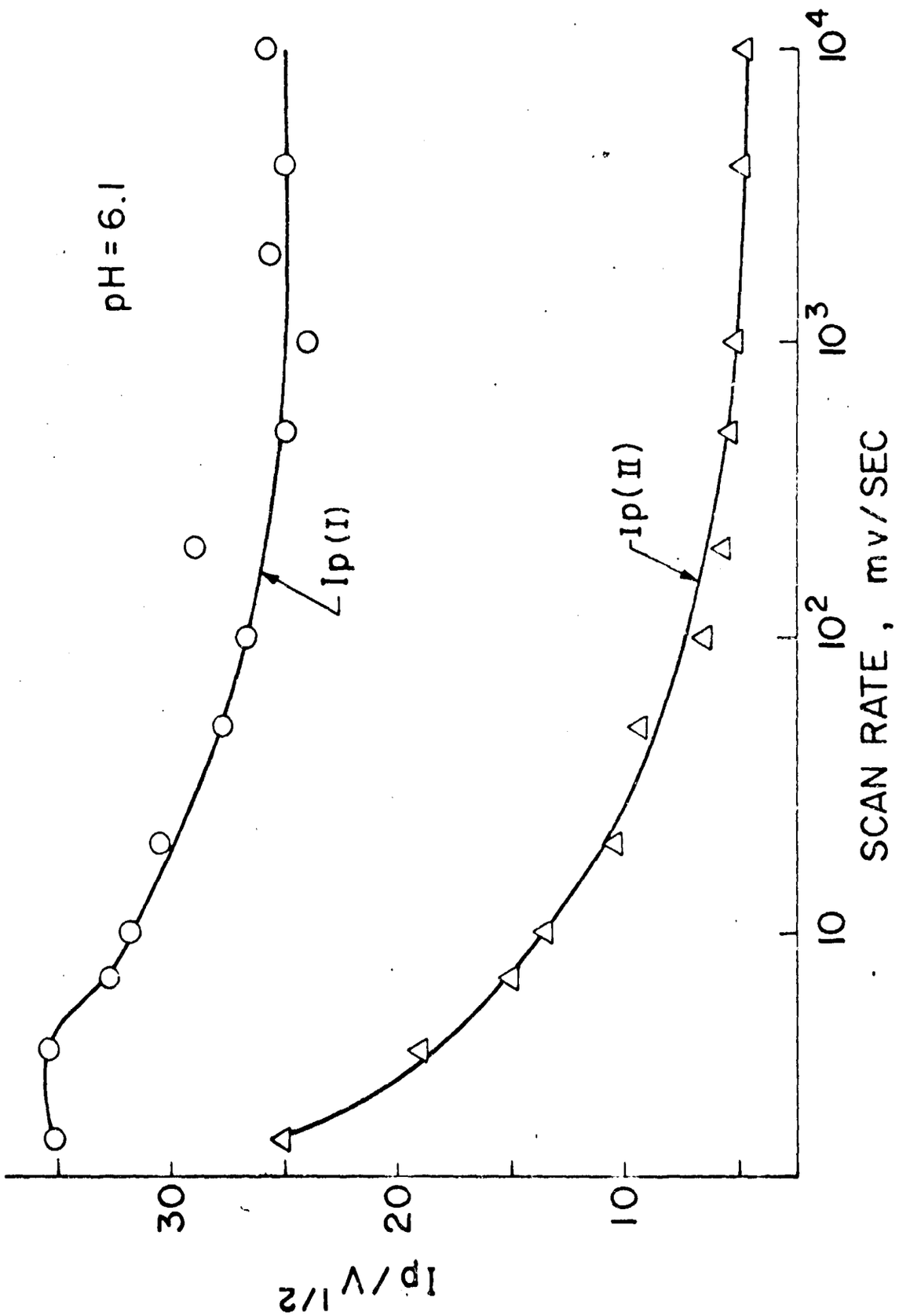

of an ECE mechanism with both electron-transfers at the same potential (or very close) or with the second charge transfer occurring at more positive potentials(second E easily reduced than the first E). These conclusions would indicate that we may be in the presence of a combination of two ECE mechanism, one including only the first step and the second one which would include both reduction steps. We may call it an ECECE mechanism (electron transfer-chemical reaction-electron transfer-chemical reaction-electron transfer) with three charge transfers and two coupled chemical reactions.

At this point of the investigation, we considered the application of other electrochemical techniques in order to confirm or rebut our previous findings. The work mainly concentrated in the first reduction step, which appeared more complicated for interpretation than the second one.

An ECE mechanism with both electron transfers at the same potential, or with the second one easier to reduce, should give typical diagrams using rotating disc electrode (RDE) and also with the potentiostatic method which apply a potential step pulse generally recognized as chronoamperometry.

In the experiments with RDE, we used exactly the same system of electrodes (PGE) and m-DNB solutions employed with cyclic voltammetry but now under hydrodynamic conditions. The disc electrodes could be rotated from 50 to 5000 rpm. Figure 22 gives some idea of the I-E curves at different rotations. Note that the definition of the two reduction waves is very well developed at low rotation rates but it becomes ill-defined as the rotation increases.

FIGURE 22. ROTATION RATE EFFECT.

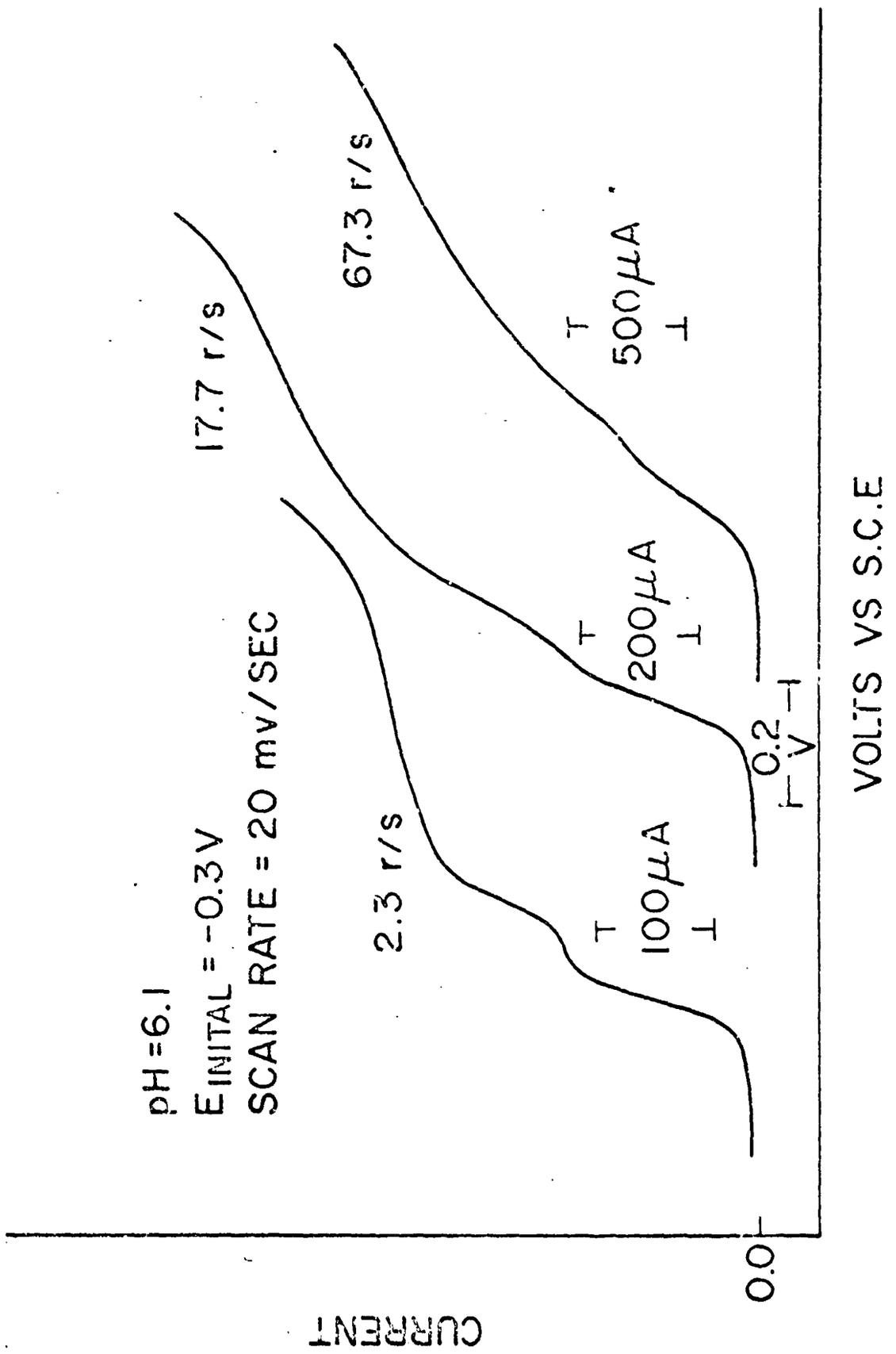

This effect is fundamentally bad with the second step and restricts the measurement of limiting current at high rotations. The reasons for this lack of normal behavior are difficult to explain but it may be attributed to the formation of the film reported before which would passivate the electrode, or for the consecutive occurrence of more than one electrode process at very close potentials.

As with cyclic voltammetry, the principal variable for electrode studies is the scan rate, using rotating electrode methods one should analyze the effect of rotation on limiting currents following the relationship of the Levich equation. Thus, the principal plot in this case, is I_{lim} vs $\omega^{\frac{1}{2}}$. Figure 23 shows this type of plot for both waves. Wave I shows a curve of I_{lim} vs $\omega^{\frac{1}{2}}$ with the characteristics expected for an ECE process. The limiting current increases with the square root of rotation but does not follow a straight line, as should be the case for a simple diffusion-convective process: its curve has a definitive different slope at low rotations than at high values, indicating that the effect of the chemical reaction in between both charge transfers is blocked as rotation increases.

Referring to the plot obtained with the second reduction step, we show only the range of rotation that permits the measurement of limiting currents. The change of the curve to a lower slope after approximately 16 rps would indicate the effect of kinetic complications, in agreement with previous findings.

The experimental data obtained from RDE technique may be used to calculate the value of the rate constant k of the chemical reaction coupled between

FIGURE 23. ROTATION RATE EFFECT

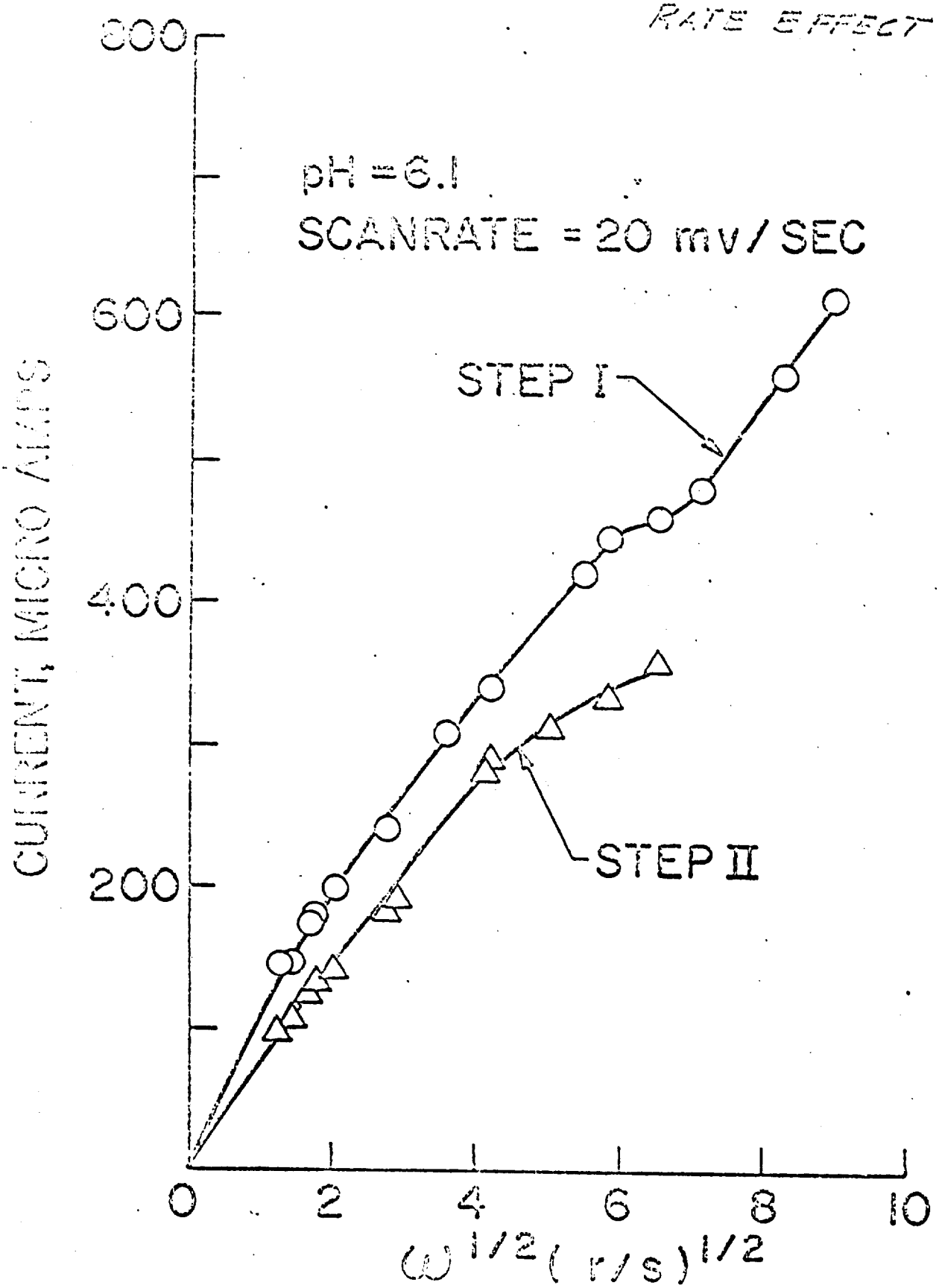

the charge transfers: Malachevsky, Marcoux and Adams[23] developed the theory for the present case. The total current is expressed by the following equation:

$$i_T = 0.62\, FA C_A^b D^{2/3} \gamma^{-1/6} \omega^{1/2} \left\{ m_1 + m_2 \left[1 - \exp\left(- \frac{0.234\, \gamma^{1/3}}{D^{1/3}} \cdot \frac{k}{\omega} \right) \right] \right\}$$

From this equation, one may see that if k is very large (∞) or $k \gg \omega$ the second term in the brackets, becomes zero and the total current is proportional to n_1+n_2. In the other limit if $k = 0$, a very slow reaction, or $k \ll \omega$ one should obtain only the effect of the first charge transfer, n_1. In practice the way to calculate k is to obtain the ratio of (i_L) obs. $/(i_L)k = 0$ at different rotations; (i_L) obs. comes from the curve and $(i_L)k = 0$ can be obtained by extrapolation from fast rotation rates. This ratio gives the following equation:

$$\frac{(i_L)_{obs}}{(i_L)_{k=0}} = 1 + \frac{m_2}{m_1} \left[1 - \exp\left(- 0.234\, \gamma^{1/3} D^{-1/3} \frac{k}{\omega} \right) \right]$$

and permits the calculation of k/ω at different rotations. Finally, by plotting k/ω vs. ω the value of k is obtained, Figure 24. For our case the value of k from the slope is equal to 13.5 sec^{-1}.

There is a third method which may provide more information about the postulated ECE process of the first reduction step. This technique is generally known as the potentiostat or chronoamperometric method. It consists in the application of a potential step to the system in equilibrium high enough to locate the potential of the electrode on the plateau of the reduction wave, and measure the transient of the current (i-t curve) on an oscilloscope. For an ECE mechanism of the type that we are considering the theory was developed by Alberts and Shain[24] and the total current should follow the following equation:

$$\frac{i_T}{FAD^{1/2} C_A^b} = \frac{m_1 + m_2 (1 - e^{-kt})}{\sqrt{\pi \cdot t}}$$

FIGURE 24. DETERMINATION OF K_1.

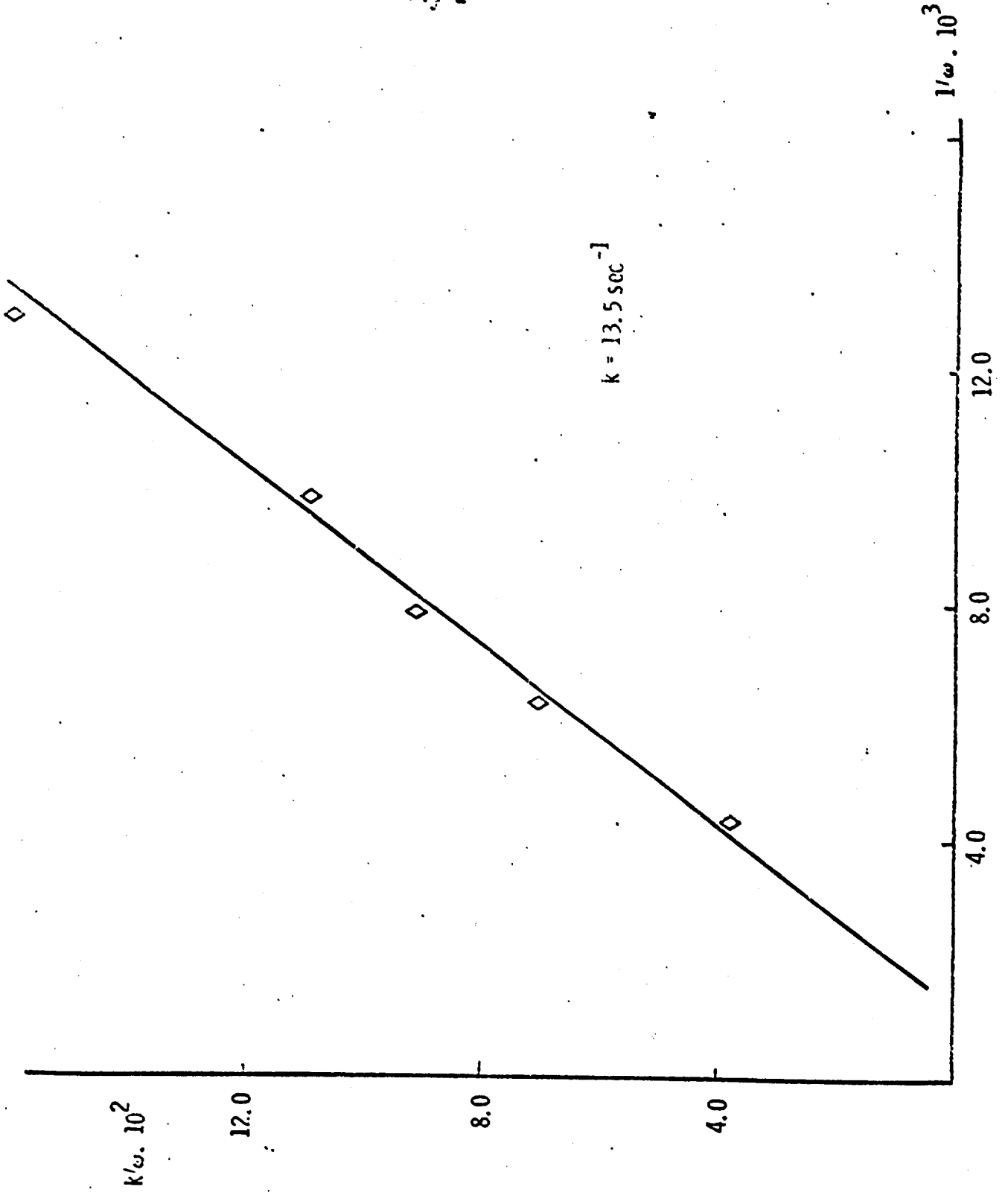

Note that in a plot of i_T vs. $1/\sqrt{t}$ if $k = \infty$, we should have the contribution of both electron transfers and for $k = 0$ only n_1 remains in the equation. This means that the plot $i_T - t^{\frac{1}{2}}$ must show a similar appearance to our previous plot of $i_L - \omega^{\frac{1}{2}}$. Unfortunately our case does not permit us to apply the potential step sufficiently negative, because the second reduction step occurs at potentials quite close to the first one, but at least these experiments may give other indications (qualitative) of the mechanism. Figure 25 is the plot ($i - t^{-\frac{1}{2}}$) of the results from the potentiostatic method. The change of slope is obtained again, following the trend expected, higher at long times when both charge transfers may occur and lower for short times when only the first electron transfer is contributing to the total current.

At this point we can summarize the results saying that by three independent electrochemical methods we have evidence that the first step of the reduction of m-DNB includes an ECE process and that the second step shows effects of a preceding chemical reaction. But what we do not know yet is if in the ECE mechanism both electron transfers occur at the same potential, or if the second is easier to reduce than the first one. To obtain the answer to the last question, the rotating ring-disc electrode seems perfectly suitable.

For example, if the ECE process has the second charge transfer at more negative potential than the first one, and if using ring-disc electrode we sweep the disc in the same manner as in the experiments with RDE and the ring is held at a potential negative to the first reduction step, we should obtain a reduction current on the ring while the first reduction is occurring. But if the case corresponds to an ECE mechanism with both electron transfers

FIGURE 25. POTENTIOSTATIC METHOD.

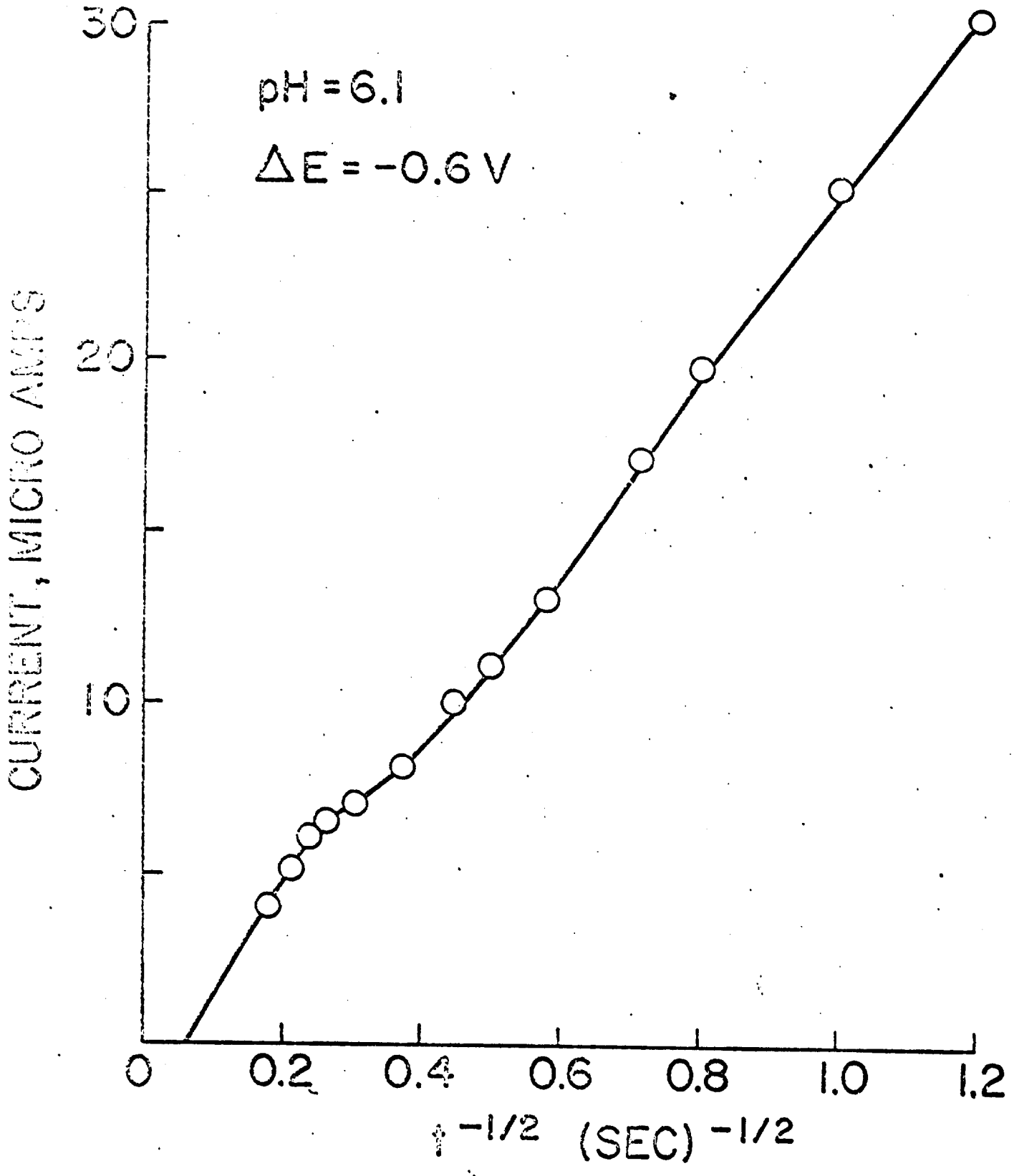

at the same potential we should not detect any current at all. Figure 26 shows these experiments and appears to demonstrate that our case corresponds to the second one because no reduction current was obtained in the potential range 0.0 to -0.35. This figure also shows the experiments with the ring held at more positive potentials. The anodic current observed at the ring corresponds to the anodic wave which we described before when discussing the experiments with cyclic voltammetry. Note how the current follows a similar pattern to the disc, and how the collection on the ring increases when this electrode is held at more and more anodic potentials. This effect is observed up to 0.7 volts vs. SCE. However, the collection efficiency (I_R/I_D) remains very low; the maximum value obtained did not reach 50% of the theoretical value and showed a decrease with increase of scan rate. What remained unclear was what the relationship was between this anodic current and the two reduction steps. Cyclic voltammetry did show that the anodic peak is obtained when one or both reduction steps were included in the scan. Now we decided that ring-disc electrode may give more information.

We ran a series of experiments that in some way are opposite to the previous experiments Figure 27. In this case, the disc was held at different potentials on convenient parts of the reduction curves and the ring was swept at 100 mv/sec from -0.3v in the anodic direction. We had intended to search for more than one anodic step related with the reduction waves. The figure shows that there is not more than one anodic step, regardless of the potentials at which the ring was held. From 0.0 to -0.4v we obtained only the residual current and at -0.5; -0.6 and -1.0v one anodic wave was developed which increased as the potential of the disc was held more negative. It is almost impossible to believe that the same product is obtained with both reduction steps. There

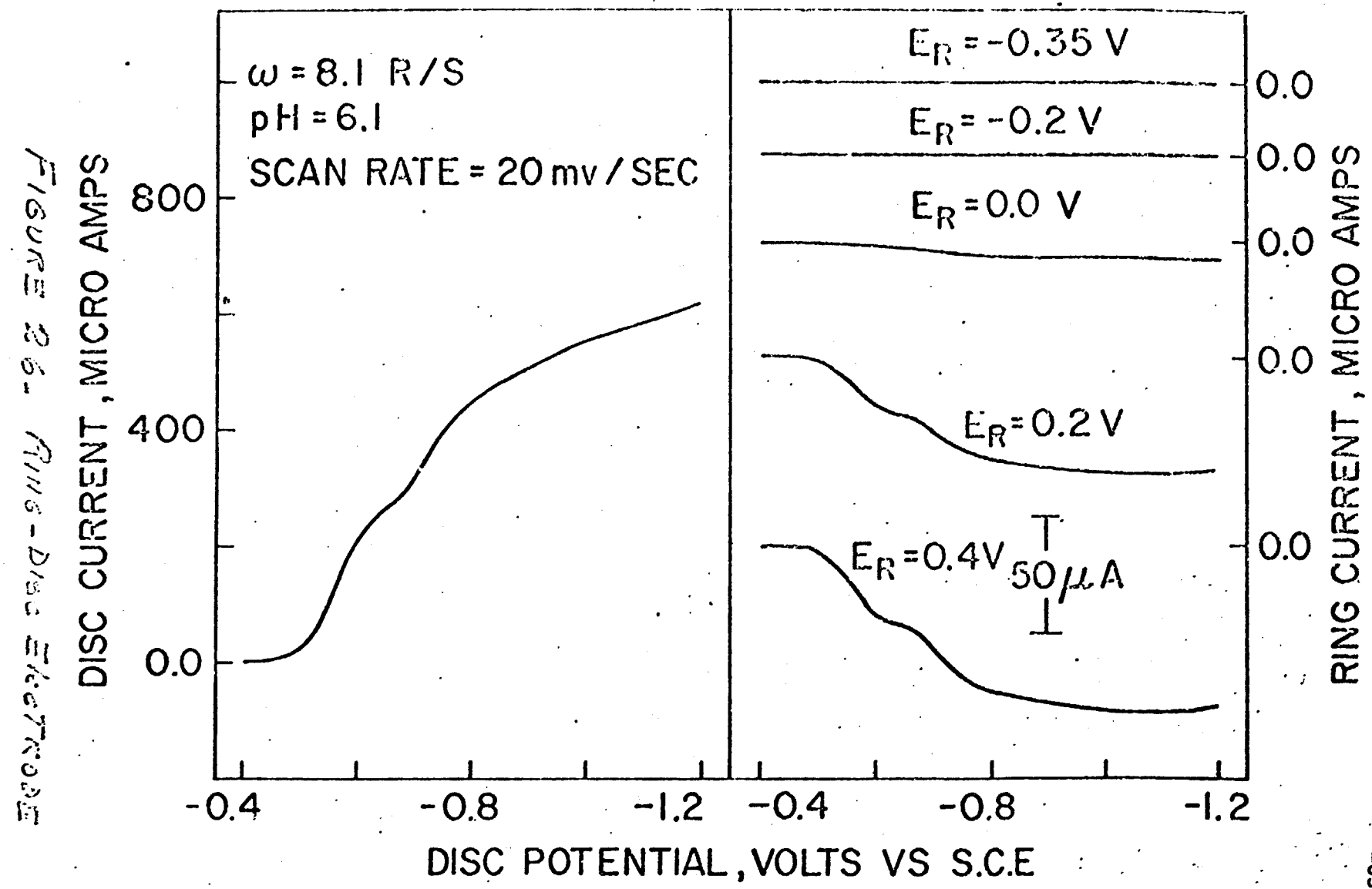
ω = 8.1 R/S
pH = 6.1
SCAN RATE = 20 mv / SEC
E_R = -0.35 V
E_R = -0.2 V
E_R = 0.0 V
E_R = 0.2 V
E_R = 0.4V
50 μA
800
400
0.0
0.0
0.0
0.0
0.0
0.0
-0.4
-0.8
-1.2
-0.4
-0.8
-1.2
DISC CURRENT, MICRO AMPS
RING CURRENT, MICRO AMPS
DISC POTENTIAL, VOLTS VS S.C.E

-63-

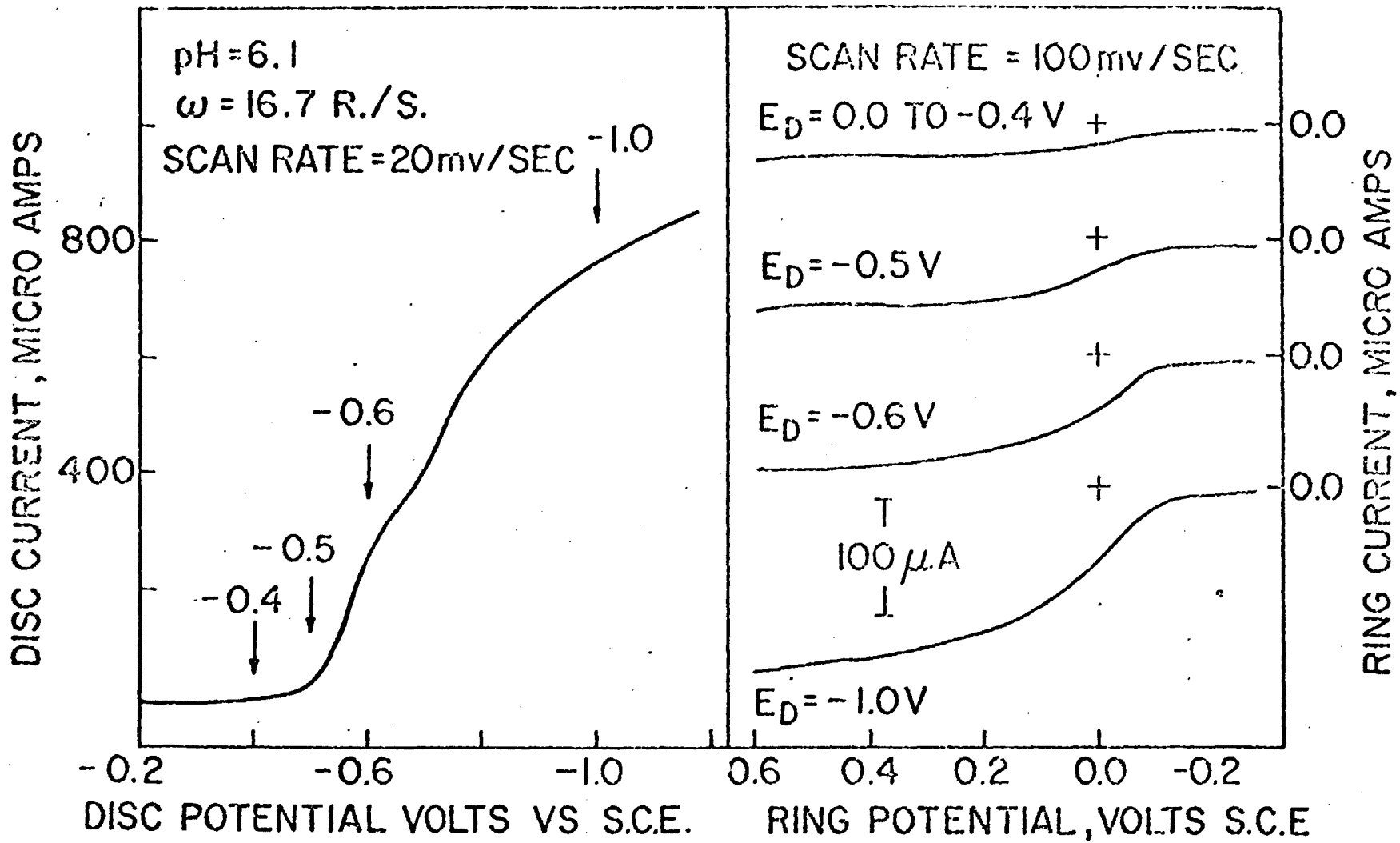
pH=6.1
ω = 16.7 R./S.
SCAN RATE=20mv/SEC
-1.0
-0.6
-0.5
-0.4
800
400
DISC CURRENT, MICRO AMPS
-0.2
-0.6
-1.0
DISC POTENTIAL VOLTS VS S.C.E.
SCAN RATE = 100mv/SEC
E_D = 0.0 TO -0.4 V
E_D = -0.5 V
E_D = -0.6 V
E_D = -1.0V
T
100 μA
0.0
0.0
0.0
0.0
RING CURRENT, MICRO AMPS
0.6
0.4
0.2
0.0
-0.2
RING POTENTIAL, VOLTS S.C.E

are several reasons that may suggest that this oxidation step is the electrode reaction of a substance (or may be more than one, which are oxidized at close potentials) which really is the product of chemical reactions following the reduction steps. Those evidences that may support this idea are, for example, the low collection efficiency obtained using the ring-disc electrode and its decrease with increase of rotation, the large separation potential between the reduction and the oxidation processes,the very low ratio between the anodic current and the cathodic currents, and the broad development of this peak.

The determination of the number of electrons participant in the electrodes processes seems very difficult as a consequence of the complexity of the mechanism. Nevertheless, using linear sweep voltammetry at very slow scan rates, the kinetics effects may be minimized. Thus, for the ECE mechanism of the first step, K becomes infinite and both electrode transfers will contribute. Referring to the second step, the preceding chemical reaction will not interfere in the production of the electroactive compound. The same idea can be applied to rotating disc electrode at slow rotations. By application of the Sevick-Randles equation and the Levich equation, making appropriate assumptions for terms unknown, such as diffusion coef. and kinematic viscosity, we obtained for the first reduction step values very close to four electrons. The second step under the same conditions gave currents on the order of 80% of the first one, which may indicate that considering the differences in parameters, it may have the same number of electrons as the first one. A second question is how many electrons are included in each charge transfer in the ECE mechanism of the first step. The ratio of plateaus in cyclic voltammetry and of slopes in RDE and potential step methods would indicate a relationship very close to 3 to 1.

Summarizing, we may express the overall mechanism in the following scheme:

Step I

$$A + n_1 e \xrightarrow{E_1'} B$$

$$B \xrightarrow{k} C$$

$$C + n_2 e \xrightarrow{E_2'} D$$

$E_1' \cong E_2'$

$n_1 = 3$

$n_2 = 1$

Step II

$$D \xrightarrow{k_2} E$$

$$E + n_3 e \xrightarrow{E_3'} F$$

$n_3 = 4$

and finally we may say that the reduction of m-DNB can follow the steps described below:

Step I

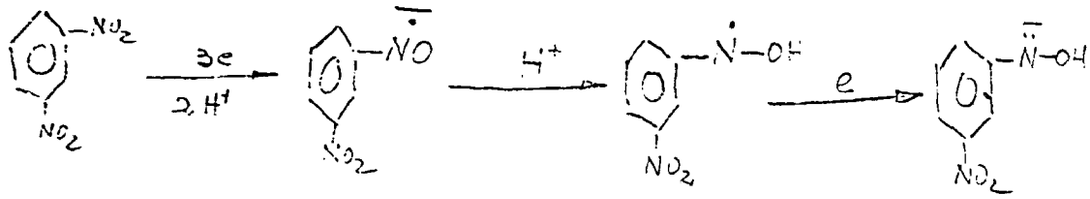

Step II

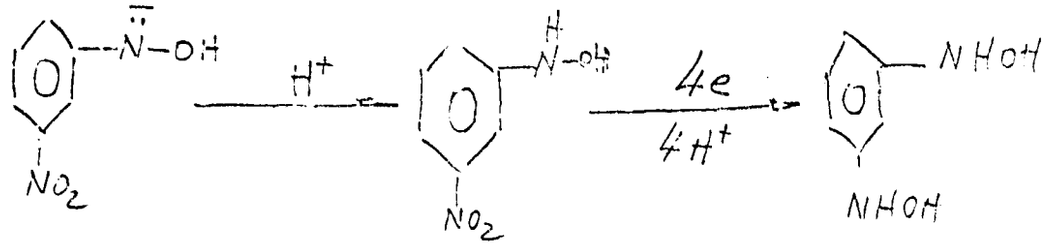

E THE ELECTROCHEMICAL OXIDATION OF ZINC METAL

This project included studies of the anodic dissolution of zinc in the active and passivated region, under well defined conditions of mass transport. Steady wire electrodes and rotating disc electrodes were used for experiments controlled by only diffusion or convective-diffusion conditions respectively. The techniques employed were: cyclic voltammetry, rotating disc electrode and rotating ring-disc electrode. In addition, we studied some aspects of the reduction behavior of the species found during the oxidation.

Experimental

The circuits described before were employed for the different techniques applied. Zinc metal 99.99% was used for the preparation of the electrodes and the solutions of KOH were prepared with analytical reagents and doubly distilled water. Two general ring-disc arrangements were used. In the first of these, a zinc ring surrounded the zinc disc and in the other the ring was constructed of pyrolytic graphite. The reason for using a zinc ring in some cases was that when amalgamated one could operate the ring at more negative potentials than graphite, before being troubled by the onset of H_2 evolution. Regardless of the nature of the ring electrode, the results to be reported here could be duplicated on either one.

Experimental Results

Figure 28 shows the effect of the point of sweep reversal on the form of the reduction curves. At the top, the dotted line shows an anodic sweep of zinc wire electrode in unstirred 1N KOH electrolyte. Here we see the

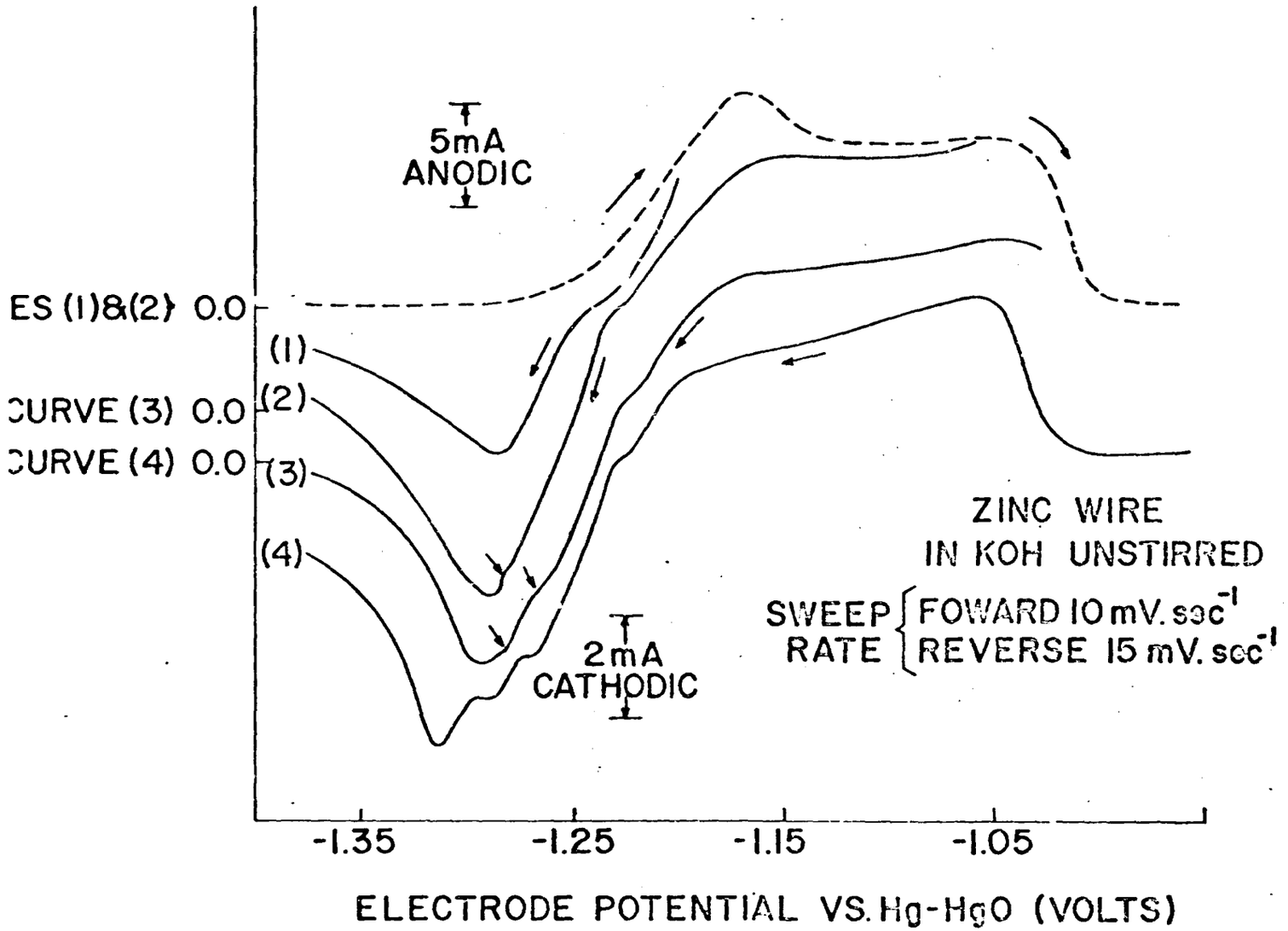
5mA
ANODIC
ES (1)&(2) 0.0
(1)
(2)
CURVE (3) 0.0
CURVE (4) 0.0
(3)
(4)
ZINC WIRE
IN KOH UNSTIRRED
SWEEP RATE
FOWARD 10 mV. sec⁻¹
REVERSE 15 mV. sec⁻¹
2mA
CATHODIC
-1.35
-1.25
-1.15
-1.05
ELECTRODE POTENTIAL VS. Hg-HgO (VOLTS)

FIGURE 6 - [illegible]

-88-

current rise to a peak at which point a film of what is presumably the hydroxide is formed on the surface which hinders further dissolution. After the peak, the current rises slowly until passivation occurs at approximately -1.02 V vs Hg/HgO. The full lines numbered 1-4 show reverse sweeps recorded at a slightly faster sweep rate for different point of sweep reversal of the anodic sweep. In curve 1 where the scan is reversed prior to the anodic peak, one observes only one large, broad reduction peak with a maximum at about -1.29V. When the sweep is reversed at a point after the peak but prior to the onset of passivation, an inflection is seen to develop on the rising part of this reduction wave, which we were unable to develop any further by variation of sweep rate, since the two reduction processes are occurring at potentials very close to one another. In curve 3, the scan was reversed just at the point where the electrode was beginning to passivate, and we can see that another inflection point has appeared at a less cathodic potential on the main reduction step. In 4, where the electrode was allowed to passivate before sweep reversal, this latter inflection is now well developed, the small inflection and the main peak have merged into a second inflection and a very pronounced peak has appeared at approximately -1.3V.

The general pattern is therefore that for a sweep terminated before the onset of passivity, one broad reduction peak is observed which incorporates that due to the reduction of the film formed in the active region and the reduction of soluble zinc species. For a sweep reversed in the passive region, two additional reduction processes appear, one at less cathodic and the other at more cathodic potentials than that of the initial broad peak.

This cathodic behavior is further illustrated in Figure 29, where we show the reduction behavior at various sweep rates for a sweep reversal in the passive region. Again, the dotted line shows the forward anodic scan to passivation with the sweep reversal commenced at -0.95V. For a return sweep of 10 mv.sec^{-1}, two well defined peaks arising from the passive film are observed with that due to the active region film and the reduction of zincate appears only as an inflection on the less cathodic peak. With increase of the scan rate, the middle peak and the most cathodic peak increased in magnitude quite markedly while the first reduction peak and the middle peak eventually merge with the most cathodic peak in the faster scan rates. This increase in the magnitude of the two most cathodic peaks must reflect the shorter time available at the faster return sweep rates for chemical dissolution of the films to occur and for dissolution products to diffuse away into the bulk of the electrolyte.

It is quite evident that removal of the passive film is not a fast process at the passivation potential since, as one can see in the figure, the electrode reactivation shifts to a more cathodic potential as the sweep rate is increased. It appears that reactivation of the electrode is permitted only after a certain amount of the film has been chemically dissolved by the electrolyte. This dependance of the reactivation process on the concentration of the electrolyte is clearly illustrated as the electrolyte concentration is decreased. At a sweep rate of 10 mv.sec^{-1} in 0.5N KOH for example, no reactivation of the electrode is observed before the reduction is reached, as a result of the extremely low rate

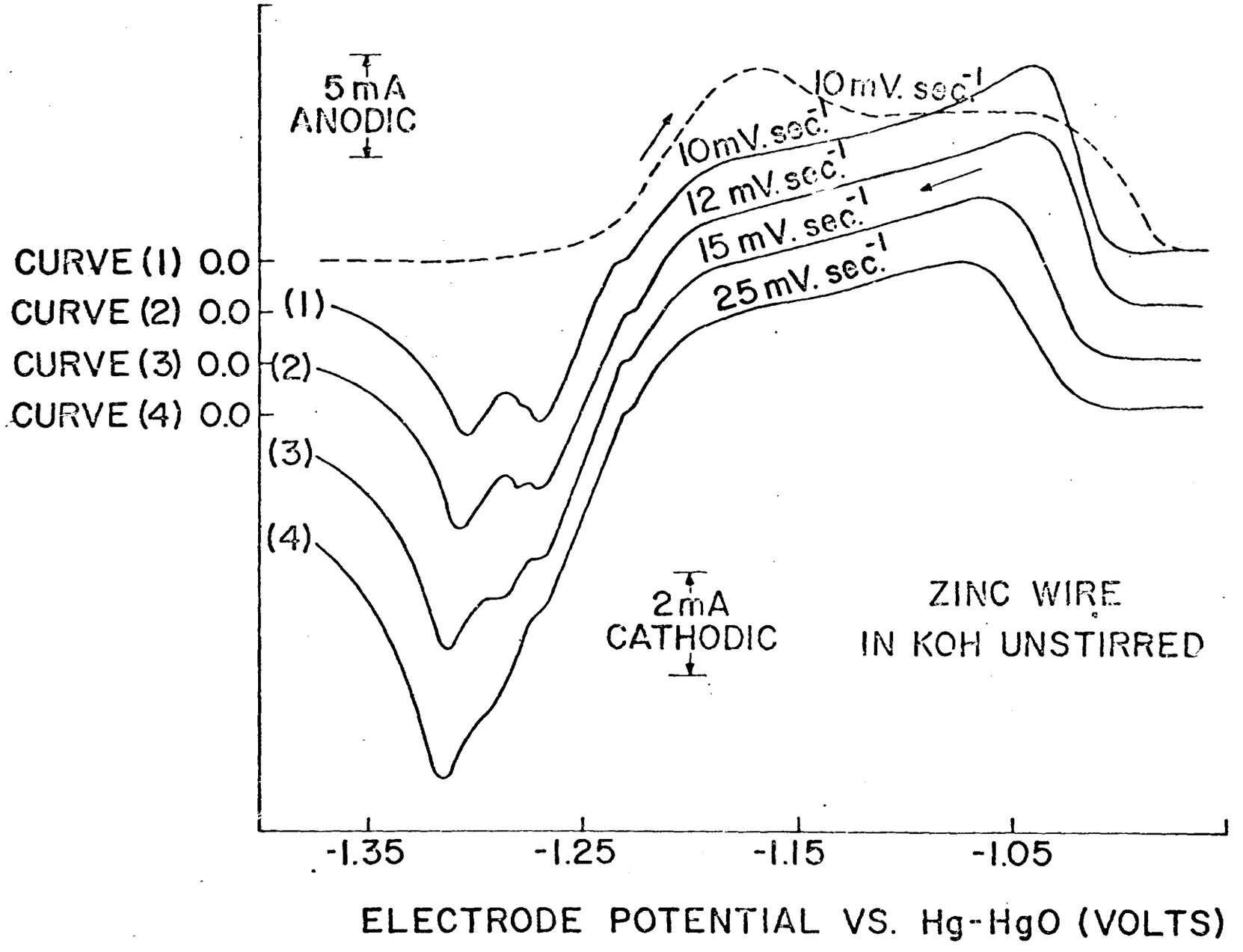
5 mA
ANODIC
10 mV. sec.-1
10 mV. sec.-1
12 mV. sec.-1
15 mV. sec.-1
25 mV. sec.-1
CURVE (1) 0.0
CURVE (2) 0.0
CURVE (3) 0.0
CURVE (4) 0.0
(1)
(2)
(3)
(4)
2 mA
CATHODIC
ZINC WIRE
IN KOH UNSTIRRED
-1.35
-1.25
-1.15
-1.05
ELECTRODE POTENTIAL VS. Hg-HgO (VOLTS)

FIGURE [illegible]

of dissolution of the passive film in this concentration of electrolyte. If, therefore, the passive film must be chemically dissolved for electrode reaction to occur, the question arises as to how the passive film gives rise to these two additional reduction peaks. One possible explanation is that not all of the passive film is dissolved off and reactivation has occurred over only a proportion of the electrode area, though this proportion increases as chemical dissolution of the film proceeds. Once the reduction region is attained, therefore, the remaining part of the passive film is reduced under the peak lying at the most cathodic potential. To explain the appearance of the peak at the least cathodic potential one may possibly suggest that this arises from that part of the passive film which was removed by chemical processes, to permit the observed electrode reactivation. This chemical process may involve, as a first step, the formation of another form of zinc hydroxide from the oxide layer, which presumably constitutes the passivating film. This hydroxide film, which need not necessarily be the same form as that produced in the active region of electrode dissolution since each is formed by a different process, can possibly give rise to this initial reduction peak. This proposal that different forms of zinc hydroxide are present on reactivated zinc electrodes would be in agreement with other investigators.[25]

Figure 30 shows the effect of sweep reversal on the same wire electrode in unstirred solution, except that the electrode has been amalgamated. One may notice in the first instance that the general level of the dissolution current is very much higher in this case. However once again at approximately -1.2V, there is a peak in the i-v curve, which on the amalgamated electrode is very much more pronounced. If the sweep is now reversed, in the potential region between this peak and the onset of passivity one sees a marked jump in the

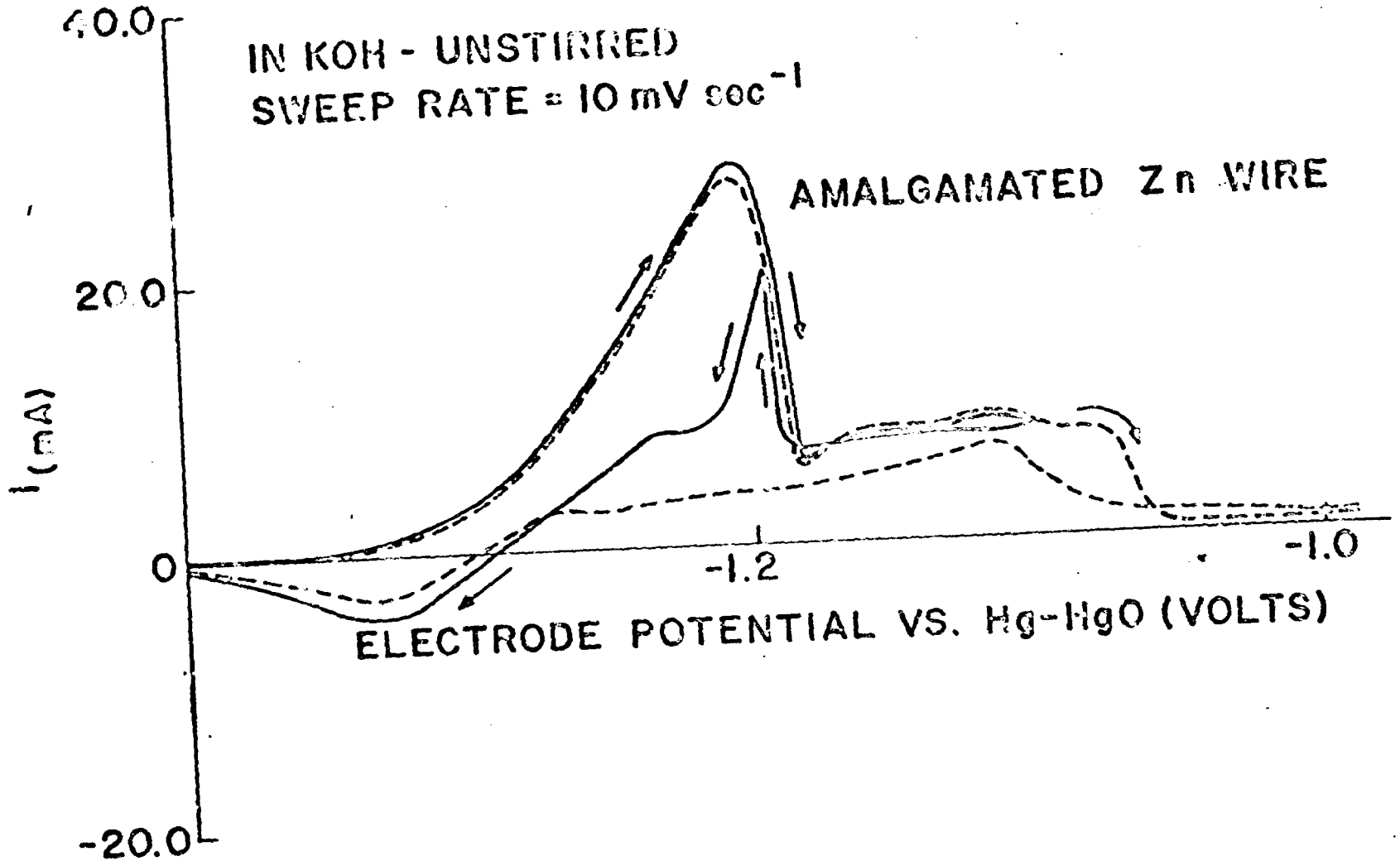
40.0
20.0
0
-20.0
I (mA)
IN KOH - UNSTIRRED
SWEEP RATE = 10 mV sec^{-1}
AMALGAMATED Zn WIRE
-1.2
-1.0
ELECTRODE POTENTIAL VS. Hg-HgO (VOLTS)

current at the peak potential as presumably the active region film disappears from the surface. Only one broad reduction peak is observed. If, however, the sweep is reversed in the passive region, a small reactivation of the electrode is observed but at the peak potential no additional rise in current is observed and the behavior of the electrode is in some way still influenced by the formation of the passive layer. In the latter case no particular influence on the passive film is seen in the reduction region, since only one broad peak is again observed, though its magnitude is lower, presumably reflecting the much lower current flowing during the active part of the return sweep in this as compared to the previous case. Thus it appears that the product remaining on the surface after the partial reactivation of the electrode is relatively insoluble and remains on the surface during the whole of the return active portion of the sweep.

This observation of formation of a film on both amalgamated and non-amalgamated electrodes at a potential of -1.2V (though a much larger current is being passed at the point in the amalgamated case) brings up the question as to whether the film is formed at this point by a dissolution-precipitation mechanism from a zincate saturated electrolyte layer on the electrode surface, or whether an absorption type mechanism is valid. This appearance and disappearance of the film at a relatively fixed potential, despite the magnitude of the current flowing across amalgamated and non-amalgamated surfaces, would appear to be in contradiction to that expected from the dissolution-precipitation model. This peak is also evidenced in stirred solutions on both forward and reverse sweeps on non-amalgamated electrodes. (Figure 31) Note in this figure how here again the peak in the forward and reverse directions is occurring at a potential of approximately -1.2 V. This type of behavior suggests that the film

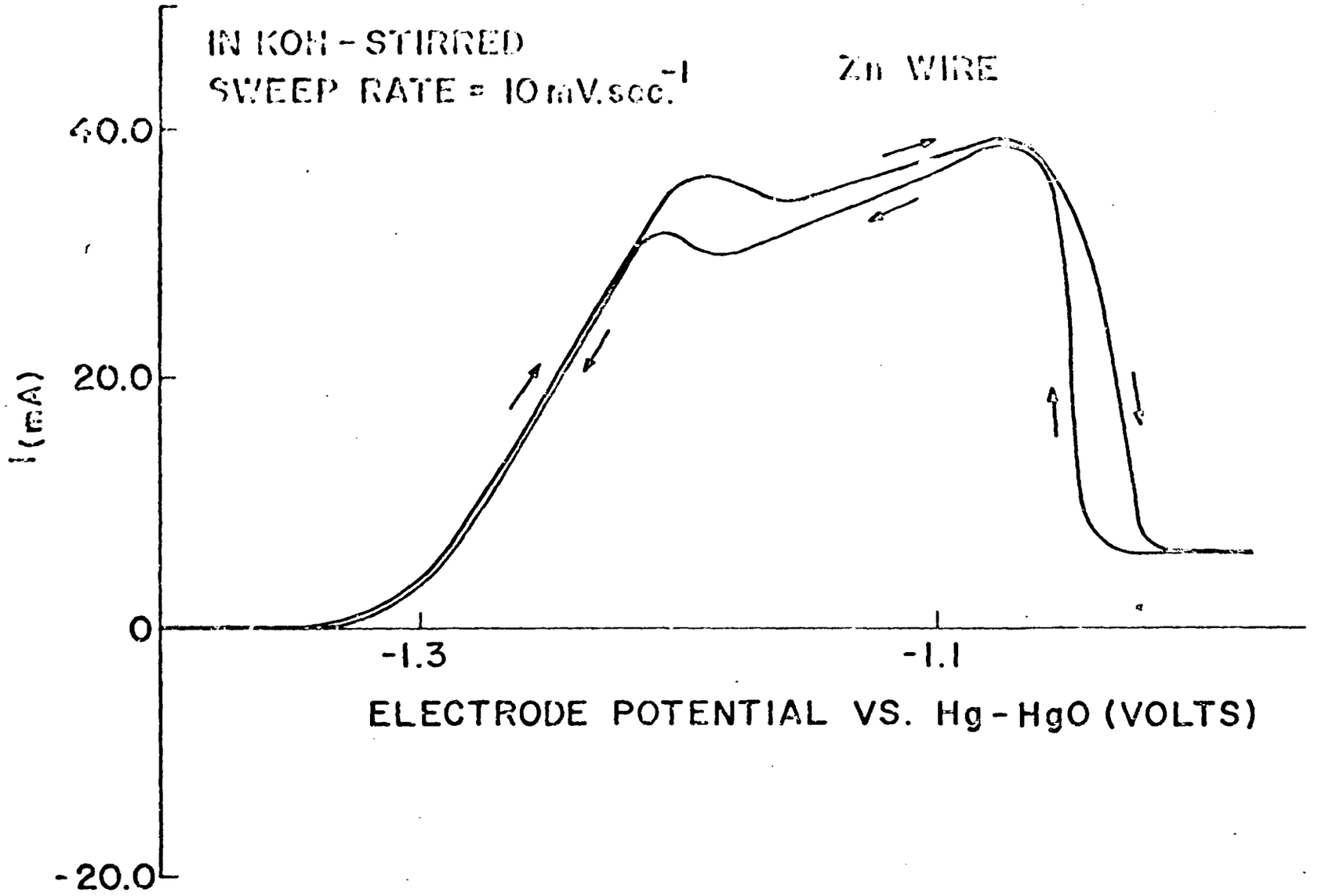

FIGURE 21 - POTENTIOGRAMMATIC ZINC - [illegible] SATURATED SOLUTIONS.

formed in the active region of dissolution is produced by the adsorption of OH^- species onto the electrode surface at a potential of about -1.2V to form a layer of $Zn(OH)_2$ and that on the reverse sweep desorption of these OH^- species occurs to leave the film detached from the surface. Before discussing these points further, it is interesting to compare the form of this curve in stirred solutions when the electrode is amalgamated. Figure 32 corresponds to this case. Here in the amalgamated case we see no peak on the forward sweep in the active region of dissolution, before the onset of passivation and one may be led to believe that no film is formed in this case in the active region. However, as we shall show later, experiments with rotating ring-disc electrodes clearly show that film does form under these conditions and can be detected from the current behavior of the ring electrode. On the reverse sweep, in spite of the greater rate of dissolution of the passive film caused by the stirring, the electrode never fully reactivated until approximately -1.1 v. Thus, the film which is preventing the dissolution, and which we propose may be some form of $Zn(OH)_2$ formed from the oxide, must be extremely tightly bound to the electrode surface. This peak at -1.1 V may arise from desorption of that hydroxide film which we believe to be formed by the adsorption mechansim at -1.2 V on the forward sweep. It has been our observation, in contrast with others, that the only conditions under which a peak is not apparent in the active region of dissolution, is when one is dealing with an amalgamated electrode, such as this, with stirring of the electrolyte. The amount of amalgamation which is required however, to cause the peak to disappear, appears to be extremely small. Traces of mercurous ions added to the cell electrolyte cause successive sweeps on an initially unamalgamated electrode to progressively change from the behavior we have indicated as characteristic of the non-amalgamated electrode to that characteristic of an amalgamated elec-

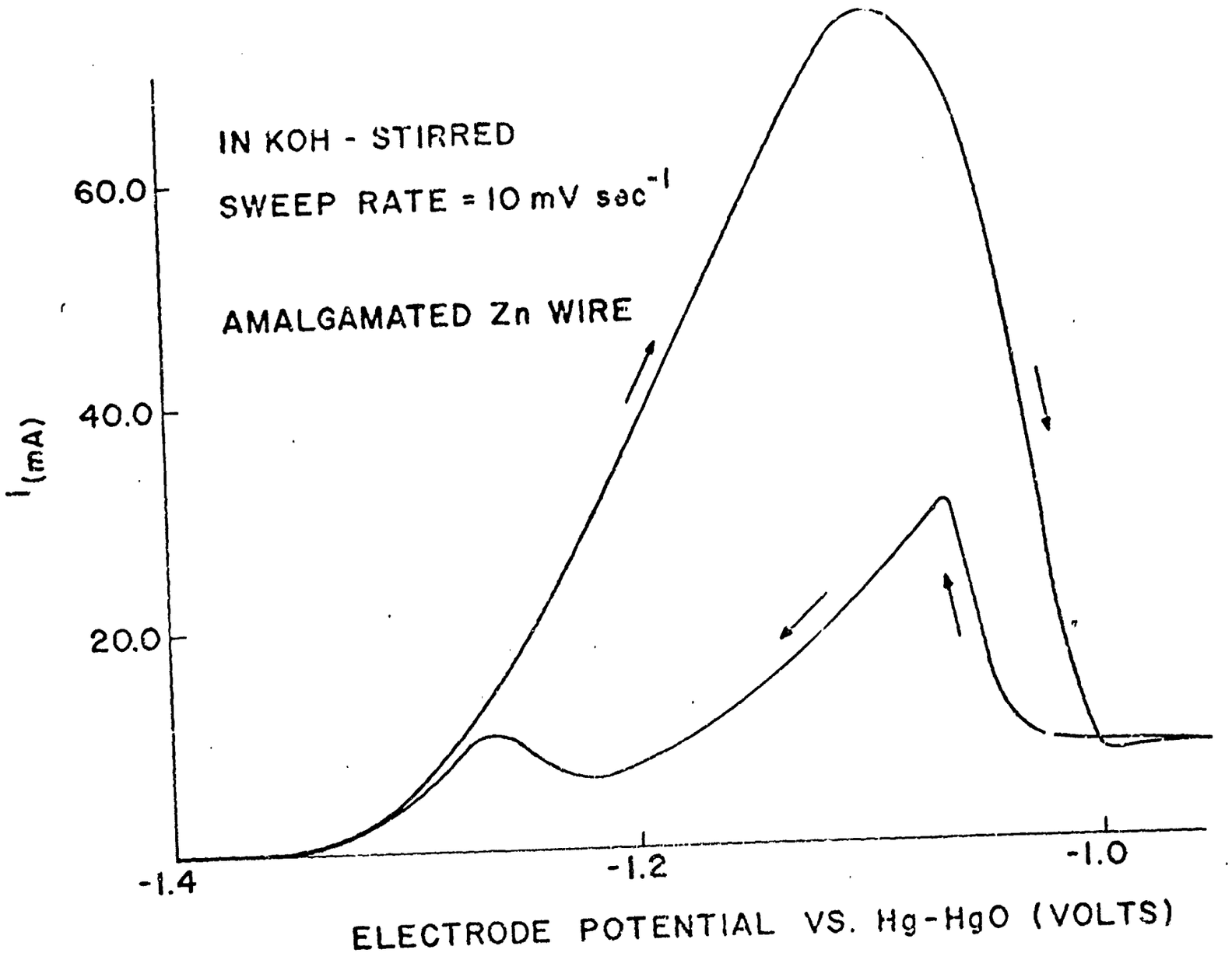
IN KOH - STIRRED
SWEEP RATE = 10 mV sec⁻¹
AMALGAMATED Zn WIRE
60.0
40.0
20.0
I (mA)
-1.4
-1.2
-1.0
ELECTRODE POTENTIAL VS. Hg-HgO (VOLTS)

trode as mercury deposits on the electrode surface. One should therefore be particularly careful in studies of this type, when using a mercuric oxide reference electrode, that contamination from this electrode is not reacting at the electrode surface.

Figure 33 shows a series of experiments using the rotating ring-disc electrode technique. In this case, we used an unamalgamated zinc disc surrounded by a zinc ring. In these experiments, the ring was held at a potential of -1.5V i.e at a potential which was sufficiently negative to completely reduce all oxidized species arriving at the ring to zinc metal. The figure shows both the disc oxidation current as a function of the disc potential, which is being varied at a rate of 10 mv. sec^{-1}, and the corresponding reduction current observed at the ring, also as a function of the disc electrode potential. Again, we can see that at each rotation speed there is a peak in the oxidation current at the disc and that this again occurs in the same potential range as before. The form of the reduction current observed on the ring closely follows that of the disc and the observed collection efficiency N is close to the theoretical value of 0.3 for all parts of the active region of dissolution both prior to and after the peak. The fact that ring current between the peak and the onset of passivity continues to rise would appear to argue against the validity of the dissolution-precipitation model for formation of the film in the active region. If, at the peak, supersaturation of the boundary layer had occurred, one would not expect the current observed on the ring to rise any further but rather perhaps to level off at a relatively constant value representative of the rate of chemical dissolution of the film by the electrolyte under the prevalent convective conditions.

FIGURE 33. RING - DISC ELECTRODE EXPERIMENTS

Our belief therefore is that the initial step in the formation of the film will proceed by the adsorption of OH^- ions onto the electrode surface at the peak potential, to give in effect a monolayer film of $Zn(OH)_2$. This film will then grow by solid state processes to an equilibrium thickness which is determined by opposing rates of film growth and chemical dissolution of the film. Thus, one might expect that at higher rotation rates, where the dissolution rates of the film is greatest, the thickness, and thus the effective resistance of the film to the passage of current, would be least. These proposals would appear to be supported by the form of the i-v curves between the peak and the onset of passivity, where their slope increases with rotation, reflecting a decrease in the film resistance and therefore a decrease in the film thickness. If the above ideas are correct, the formation of the film which causes passivity is unlikely to be formed by a dissolution-precipitation process. Our view in regard to this is that the layer of OH species adsorbed on the electrode surface undergoes a deprotonation reaction to leave the surface covered with what is effectively a layer of oxygen ions and that the remaining layers of zinc hydroxide are dissolved off in the early stages of the passive region while a non-faradaic thickening of this underlying oxide layer occurs.

If we now consider the variation of the peak current with rotation one would expect that if dissolution-precipitation does occur, then this point represents a critical concentration of dissolved zinc species at the inner boundary of the diffusion layer adjacent to the electrode surface. Furthermore, one would expect that since the current at this point would reflect the rate of diffusion of these zinc species into the bulk of the solution that this current at the peak would vary linearly with the square root of

rotation. As Figure 34 shows, this is not observed to be the case. At the lowest rotation rates, below 600 rpm, one could possibly assume linearity but above this and up to values of 5000 rpm it is quite obvious that there is a leveling off in the peak current with rotation. Thus, one must conclude that the concentration of soluble zinc species at the electrode surface, when the peak has been reached, does not have a constant value at different rotation rates.

This evidence thus argues strongly against the dissolution-precipitation model for formation of the film. A similar plot is obtained if one plots the maximum current prior to passivation as a function of $\omega^{\frac{1}{2}}$ which will rule out dissolution-precipitation for this film also. In Figure 35 we show the collection efficiencies as they can be obtained from a plot of disc current vs ring current. There are experiments with both amalgamated and non-amalgamated zinc ring-disc electrodes at a series of rotation rates. If one studies the non-amalgamated series first, one can see the constancy of the collection efficiency over the whole of the active region of the dissolution. The slope is the same after the peak has been formed, which would indicate that if any thickening of the film does occur it must be extremely little (since this would cause a drop in the amount of dissolution products arriving at the ring) and hence causes a drop in N. The amalgamated case is slightly different. We showed before how an amalgamated zinc wire showed no evidence of peak behavior in stirred electrolytes during the active portion of the dissolution process. We found the same type of behavior for an amalgamated zinc disc. However, the ring current in this case does betray the formation of a film on the disc by the sharp change in slope of the collection efficiency N, as shown in the three cases at different

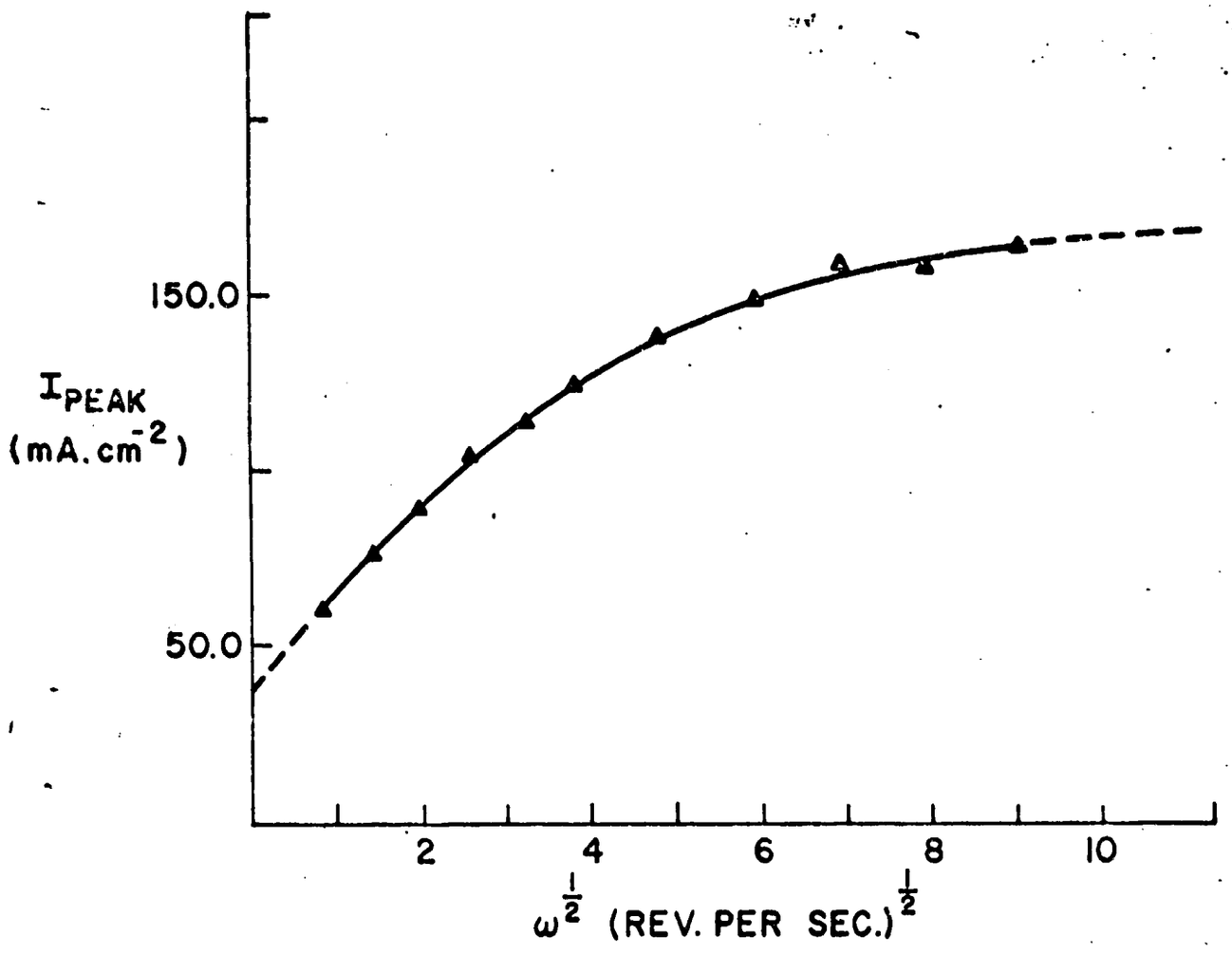

FIGURE 34. EFFECT OF ROTATION RATE ON PEAK CURRENT

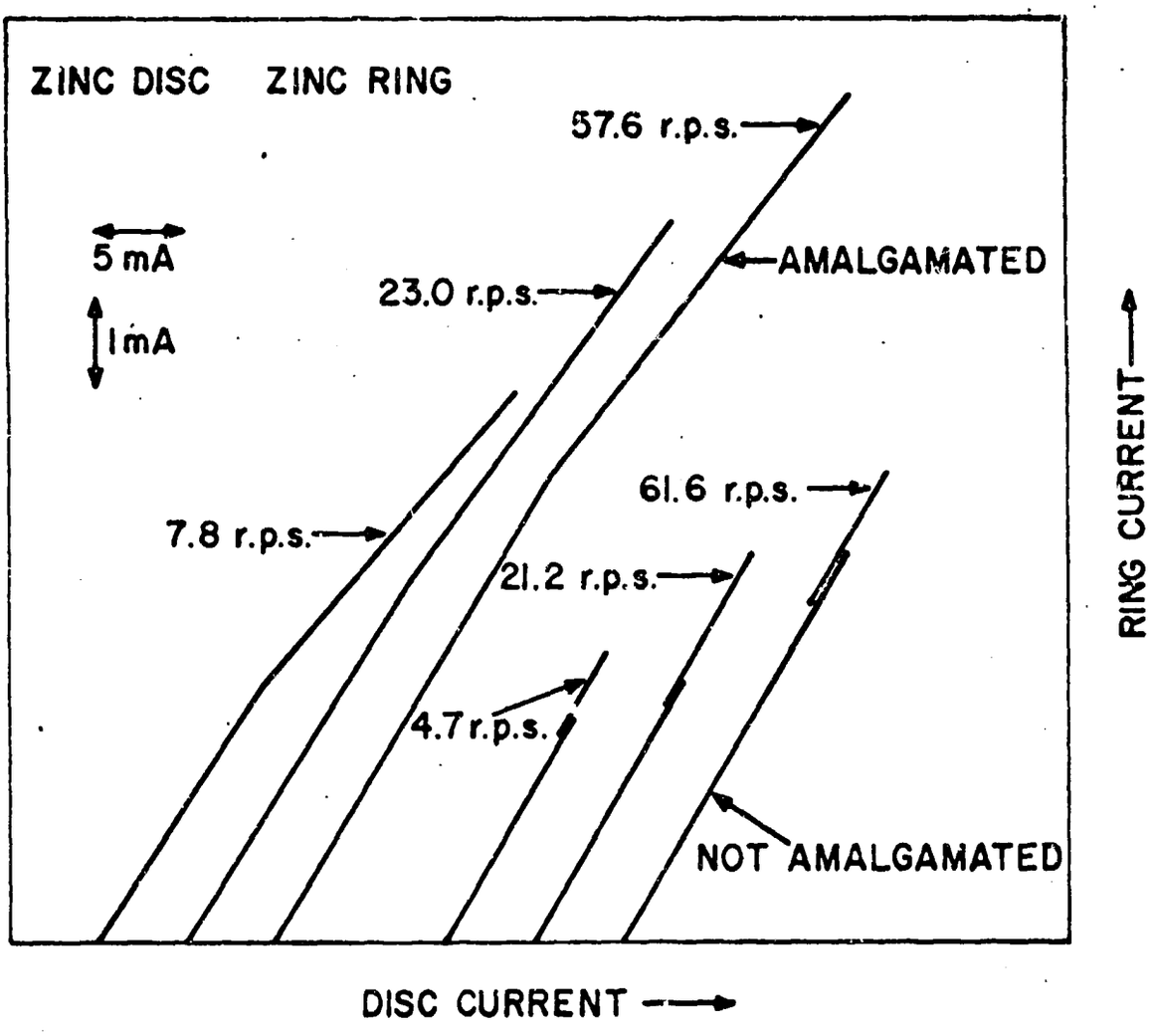

FIGURE 35. COLLECTION EFFICIENCY OF AMALGAMATED AND NON-AMALGAMATED ELECTRODES.

rotation rates.

At present we believe that the observed change in the slope of N, in the amalgamated case, in contrast with the observed constancy of the slope in the non-amalgamated case, may be explained by the difference in the degree of adherency of the hydroxide film to the surface. In the amalgamated case it seems plausible to reason that the degree of adherency is much less and hence the film can be flaked off from the surface by the rigorous electrolyte flow and escapes detection by the ring. As the film flakes it must be constantly replenished on the surface, and by this process a certain amount of the species oxidized at the disc escapes detection by the ring, and N falls.

We therefore believe that these results are quite firm evidence for the formation of the film in the active region, on both amalgamated and non-amalgamated electrodes, by a mechanism involving adsorption of OH^- species on the surface once a certain critical potential is exceeded, rather than by precipitation from soluble species in the immediate vicinity of the electrode surface. Furthermore, we suggest that our data also indicate that the passive film is formed from this initial layer of adsorbed hydroxide by elimination of the proton at the potential of passivation and not by a process of precipitation.

Finally, we would like to include some experiments related to one aspect of the film formation in the passive region up to the onset of oxygen evolution. The following Figure 36 shows the anodic current on the disc and the corresponding reduction current on the ring held at -1.7V. It is in this region

FIGURE 35 - PASSIVE REGION

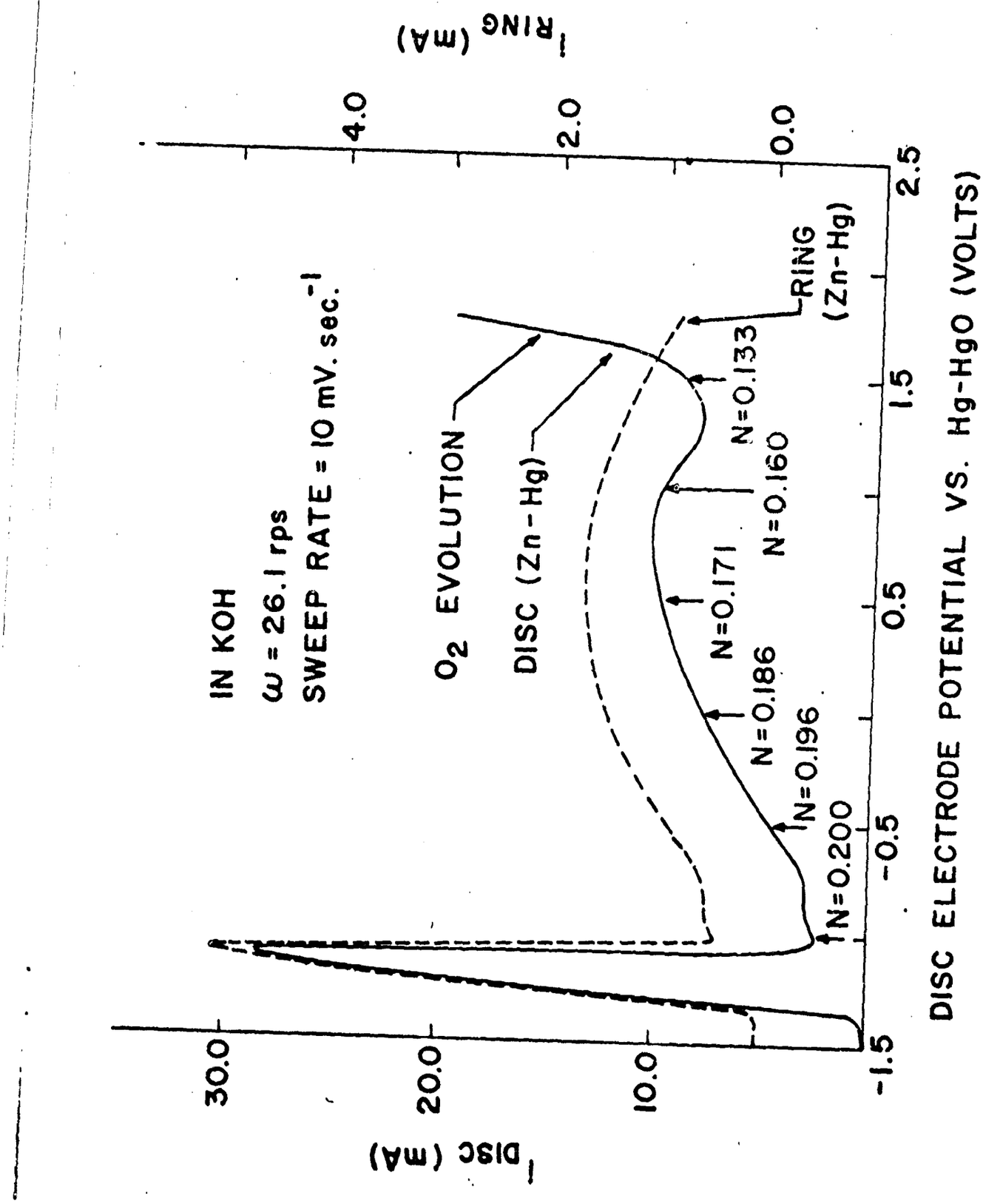

only of I-v curves that one sees evidence from this technique of what might be a film thickening process. As one can see, the collection efficiency drops steadily from the onset of passivation until the onset of O_2 evolution, although the continued deposition of zinc on the ring has the general tendency to cause the collection efficiency to rise. On the other hand, on the reverse sweep, the disc current shows a sudden jump. Paralleling this jump, the ring current shows a sharp, short decrease. This effect may be an indication that there may be a higher oxide than ZnO formed during the forward sweep, and that the fall in $\underline{N}$ on the forward sweep is related to the formation of these higher oxides.

F DISSOLUTION RATE MEASUREMENT

The ring-disc technique shows promising advantages for the determination of dissolution rates of substances and consequently to the extention of corrosion rate measurements. If the disc of a conventional ring-disc electrode is made with the substance of which one wishes to determine the dissolution rate, and the ring is an inert electrode which can be controlled at a potential capable of oxidizing or reducing the products of the dissolution, the rate of the dissolution process may be measured.

It was found that the dissolution rate constant k_s is directly proportional to the square root of rotation. $k_s = \alpha \omega^{1/2}$

where $\alpha = 0.62 D^{2/3} \gamma^{-1/6}$

The proportionality constant α, which includes the diffusion coefficient D and the kinematic viscosity γ, can be determined experimentally. The ring electrode of an electrode assembly is used for evaluation of α. The value may be calculated from limiting currents (i_R) at different rotations, using a solution of known concentration of the substance under study without the necessity of knowing previously D and γ.

Other derived expressions relate the dissolution rate $\frac{dN}{dt}$, with current at the ring i_R, and surface concentration C_s (or saturation concentration) with i_R

$$\frac{dN}{dt} = \frac{O}{zFAN} \cdot i_R$$

$$C_s = \frac{i_R}{\alpha z FAN} \cdot 1/\omega^{1/2}$$

Where

O = disc area
z = number of electrons
F = Faraday
A = ring area
N = collection efficiency

REFERENCES

1. H. Gerischer and W. Vielstich, Z. Phys. Chem. (N.F.) 3, 16, (1955) 4, 10, (1955).

2. W. Vielstich and P. Delahay, J. Am. Chem. Soc. 79, 1874, (1957).

3. W. M. Smit and M. D. Wijnen, Rec. Trav. Chim. 79, 5, 203, 289, (1960).

4. T. Berzins and P. Delahay, J. Am. Chem. Soc. 77, 6448, (1955).

5. M. D. Wijnen and W. M. Smit, Rec. Trav. Chim. 79, 22, 203, 189, (1960).

6. H. Gerischer and M. Krause, Z. Phys. Chem. (N.F.) 10, 264, (1957); 14, 184, (1958).

7. H. Matsuda, S. Oka and P. Delahay, J. Am. Chem. Soc. 81, 5077, (1959).

8. P. Delahay, J. Phys. Chem. 66, 2204, (1962); P. Delahay and A. Armata, J. Phys. Chem. 66, 2208, (1962).

9. F. C. Anson, Anal. Chem. 38, 1924, (1966).

10. J. E. B. Randles, Disc. Far. Soc. 1, 11, (1947); J. E. B. Randles and K. W. Somerton, Trans. Far. Soc. 48, 937, 951, (1952).

11. H. Gerischer, Z. Phys. Chem. (N.F.) 1, 278, (1954).

12. D. C. Grahame, J. Electro-chem. Soc. 99, 370 C, (1952).

13. A. A. Pilla, in press, J. Electro-chem. Soc 117, (1970).

14. F. B. Hildebrand, Advanced Calculus for Applications, Prentice-Hall, Inc., (1962)

15. P. Delahay, Advances in Electro-chemistry and Electro-chemical Engineering, P. Delahay, Ed., Interscience, N. Y. (1961). Vol.1, P. 278.

16. J. H. Sluyters, et. al., Rec. Trav. Chem. 82, 525, 553, (1963).

17. D. E. Smith, Electro-analytical Chemistry, A. J. Bard, Ed., Marcel Dekker, N. Y. Vol. 1, P. 1.

18. B. P. Piggin, Ph.D. Thesis - Univ. of Southhampton, 1967.

19. J. Pearson, Trans. Faraday Soc. 44, 683, (1948).

20. G. W. Jackson and J. S. Dereska, J. Electro-chem. Soc. 112, 1218, (1965).

REFERENCES Cont'd.

21. A. L. Endrey and T. A. Reilly, Power Sources Conf. 22, 91, (1968).

22. R. N. Adams, Anal. Chem. 30, 1576, (1958).

23. P. Malachevsky, L. S. Marcoux and R. Adams, J. of Phys. Chem. 70, 4068, (1966).

24. G. Alberts and I. Shain, Anal. Chem. 35, 1859, (1963).

25. Z. Ya Nikifima, J. Applied Chem. (USSR) 31, 209, (1958).

Security Classification

DOCUMENT CONTROL DATA - R & D

(Security classification of title, body of abstract and indexing annotation must be entered when the overall report is classified)

1. ORIGINATING ACTIVITY (Corporate author)

Battery Corporation of America
43 West Front Street
Red Bank, New Jersey

2a. REPORT SECURITY CLASSIFICATION

Unclassified

2b. GROUP

3. REPORT TITLE

TRANSIENT METHODS FOR ANALYSIS OF ELECTROCHEMICAL KINETICS

4. DESCRIPTIVE NOTES (Type of report and inclusive dates)

Final 1 Oct 68 to 30 Sept 69

5. AUTHOR(S) (First name, middle initial, last name)

Jorge E. A. Toni

6. REPORT DATE

DECEMBER 1969

7a. TOTAL NO. OF PAGES

7b. NO. OF REFS

8a. CONTRACT OR GRANT NO.

DAA307-69-C-0056

b. PROJECT NO. 1T0 61102 A 34A

c. Task No. -02

d. Subtask No. -36

9a. ORIGINATOR'S REPORT NUMBER(S)

9b. OTHER REPORT NO(S) (Any other numbers that may be assigned this report)

ECOM-0056-F

10. DISTRIBUTION STATEMENT

This document has been approved for public release and sale; its distribution is unlimited.

11. SUPPLEMENTARY NOTES

12. SPONSORING MILITARY ACTIVITY

Commanding General
US Army Electronics Command
Fort Monmouth, N.J. ATTN: AMSEL-KL-PF

13. ABSTRACT

Perturbation of the equilibrium state of electrochemical systems included the following techniques: relaxation methods, techniques with linearly varying potential, hydrodynamic methods (under well controlled forced correction) and techniques employing carbon paste electrodes of insoluble electroactive materials.

The final report includes a review of relaxation methods and describes the principal achievements in the following areas: Instrumentation: Two new circuits for the independent control of two working electrodes (ring-disc assemble) in the same electrolyte are described; Characterization of mercury batteries by pulse techniques: It was proved that pulse methods can give promising results concerning the state of charge of mercury batteries; Electroreduction of m-dinitrobenzene: The mechanism of m-DNB reduction in $Mg(ClO_4)_2$ solution correspond to an ECECE mechanism. An electrode mechanism consistent with the experimental data was postulated; Oxidation of zinc anode: The evaluation of oxidation and reduction processes of zinc gave supporting data for an "adsorption model" instead of the classical "dissolution-precipitation model" assigned to the passivation of zinc anode; Dissolution rate measurement: Utilizing the rotating ring-disc electrode concept, a new theory for the measurement of dissolution and corrosion rates was developed.

DD FORM 1 NOV 65 1473 REPLACES DD FORM 1473, 1 JAN 64, WHICH IS OBSOLETE FOR ARMY USE.

Security Classification

14. KEY WORDS	LINK A		LINK B		LINK C	
	ROLE	WT	ROLE	WT	ROLE	WT
Electrochemistry						
Electrodekinetics						
Battery Electrodes						
Batteries						
Transient						
Zinc						
Mercury						
Meta-dinitrobenzene						
Rotating disc						
Diffusion						
Convection						
Potentiostat						
Impedance						
Reference Electrode						
Voltammetry						
Dissolution						
Passivation						